NACA RM L51K26

NACA

RESEARCH MEMORANDUM

FORCE AND PRESSURE INVESTIGATION AT LARGE SCALE OF A 49° SWEPTBACK SEMISPAN WING HAVING NACA 65A006 SECTIONS AND EQUIPPED WITH VARIOUS SLAT ARRANGEMENTS

By Stanley Lipson and U. Reed Barnett, Jr.

Langley Aeronautical Laboratory
Langley Field, Va.

CLASSIFICATION CANCELLED

Authority Crowley Date 12-11-53

By T. C. F. Release form no. 1834

NATIONAL ADVISORY COMMITTEE FOR AERONAUTICS

WASHINGTON

January 29, 1952

NATIONAL ADVISORY COMMITTEE FOR AERONAUTICS

RESEARCH MEMORANDUM

FORCE AND PRESSURE INVESTIGATION AT LARGE SCALE OF A 49° SWEPTBACK SEMISPAN WING HAVING NACA 65A006 SECTIONS AND EQUIPPED WITH VARIOUS SLAT ARRANGEMENTS

By Stanley Lipson and U. Reed Barnett, Jr.

SUMMARY

An investigation has been conducted to determine the effect of varying the span and deflection angle of a 15-percent-chord slat on the longitudinal aerodynamic characteristics of a semispan wing having 49.1° of sweepback at the leading edge, an aspect ratio of 3.78, a taper ratio of 0.586, and incorporating NACA 65A006 airfoil sections streamwise. In addition to force measurements, chordwise pressure distributions were obtained on the wing and extended slat with and without a deflected trailing-edge flap. The tests were conducted in the Langley full-scale tunnel with the greater part of the data being obtained at a Reynolds number of 6.1×10^6 and at a Mach number of 0.10.

The results indicate that, from static longitudinal stability considerations, a slat span of 0.50 wing semispan was the most effective, for the subject wing, of the configurations investigated; that slat spans shorter than 0.625 wing semispan had no effect on maximum lift; and, at a given lift coefficient, increasing the slat span and/or slat deflection up to 45° reduced the drag characteristics of the wing in the moderate- and high-lift range.

INTRODUCTION

The usefulness of slats in improving the low-speed characteristics of sweptback wings has been demonstrated in several investigations of specific high-speed plan forms. (See, for example, references 1 and 2.) Inasmuch as the flow characteristics for a sweptback wing change considerably with variations in wing sweep and airfoil profile, the stall-control-device requirements (both aerodynamic and structural) for sweptback wings will also vary with wing geometry.

In order to augment the limited amount of available low-speed, large-scale, slat data on swept wings, an investigation was conducted in the Langley full-scale tunnel of a 15-percent-chord slat on a semi-span 49.1° sweptback wing. The wing has an aspect ratio of 3.78 and incorporates NACA 65A006 airfoil sections streamwise. The longitudinal force characteristics of the wing were obtained for several slat spans and deflection angles. In addition, chordwise pressure distributions were determined from pressure orifices located on the wing and on the extended slat. Most of the data were measured at a Reynolds number of 6.1×10^6 and at a Mach number of 0.10.

COEFFICIENTS AND SYMBOLS

The test data are presented as standard NACA coefficients of forces and moments. The data are referred to a set of axes coinciding with the wind axes, and the origin was located at the quarter-chord point of the mean aerodynamic chord.

C_L lift coefficient $\left(\frac{\text{Twice model lift}}{q_o S}\right)$

$C_{L_{max}}$ maximum lift coefficient

C_D drag coefficient $\left(\frac{\text{Twice model drag}}{q_o S}\right)$

C_{D_o} profile drag coefficient

C_m pitching-moment coefficient about the quarter-chord point of the mean aerodynamic chord $\left(\frac{\text{Twice model pitching moment}}{q_o S \bar{c}}\right)$

c_{n_s} slat-section normal-force coefficient $\left(\int_0^1 P_r \, d\left(\frac{x}{c_s}\right)\right)$

A aspect ratio (b^2/S)

b twice model span, feet

c local wing chord measured parallel to plane of symmetry, feet

c_s local slat chord measured parallel to plane of symmetry, feet

c' local wing chord measured perpendicular to 0.50c' line (see fig. 1), feet

c'_f local trailing-edge flap chord measured perpendicular to 0.50c' line, feet

c'_s local slat chord measured perpendicular to 0.50c' line, feet

$\bar{c}$ mean aerodynamic chord, feet $\left(\frac{2}{S}\int_0^{b/2} c^2 dy\right)$

P_r $P_{\text{lower wing surface}} - P_{\text{upper wing surface}}$

P pressure coefficient $\left(\frac{p - p_o}{q_o}\right)$

p local static pressure, pounds per square foot

p_o free-stream static pressure, pounds per square foot

q_o free-stream dynamic pressure, pounds per square foot $\left(\frac{\rho V^2}{2}\right)$

R Reynolds number $\left(\frac{\rho V \bar{c}}{\mu}\right)$

S twice model area, square feet

V free-stream velocity, feet per second

x chordwise coordinate parallel to plane of symmetry, feet

x' chordwise coordinate measured perpendicular to 0.50c' line, feet

y spanwise coordinate perpendicular to plane of symmetry, feet

y_{cp} spanwise location of the wing center of pressure, percent $\frac{b}{2}$

α angle of attack, degrees

δ_s angle of deflection of slat, degrees

ρ mass density of air, slugs per cubic foot

μ coefficient of viscosity, slugs per foot second

MODEL

The wing was tested as a semispan configuration mounted on a reflection plane in the Langley full-scale tunnel as shown in figure 2. A complete description of the reflection-plane construction and the wind-tunnel flow characteristics in its vicinity are presented in reference 3.

The wing had 49.1° of sweepback at the leading edge, an aspect ratio of 3.78, a taper ratio of 0.586, and no geometric dihedral or twist. The streamwise airfoil section was an NACA 65A006 section with the extreme tip of the wing being half of a body of revolution based on the same section ordinates. The wing plan form and some of the more pertinent dimensions are presented in figure 1.

As may be noted from the wing layout of figure 1, a special significance is attached to the 0.50c' line. The mounting system of the subject wing was designed such that the sweepback angle of the wing may be varied and the pivot point of the arrangement is located on the 0.50c' line. The choice of this particular chord line for the pivot point was from mechanical rather than from aerodynamic considerations. The 0.50c' line was then employed as the reference chord line for layout purposes of the flap dimensions, pressure-tube installations, and so forth, since percentages of chord lengths normal to the 0.50c' line remain constant regardless of the angle of sweepback at which the wing is being tested.

Details of the arrangement employed for the investigation of a 15-percent-c' slat are presented in figure 3. The ordinates of the slat are derived from those of the wing airfoil so that the slat could feasibly be retracted into a wing of the dimensions tested herein. For the present investigation, however, the slat was not constructed as an integral part of the wing and is mounted directly onto the unmodified basic-wing leading edge with the slat brackets alined normal to the wing's leading edge. The slat was composed of several individual spanwise segments so that slat spans of 0.250b/2, 0.375b/2, 0.500b/2, 0.625b/2, 0.750b/2, and 1.000b/2 could be obtained. All the slat tests were conducted with the outboard end of the slat located at the wing tip. The minimum chordwise clearance between the slat and wing, and the distance of the slat nose ahead of the wing were selected from the slat-positioning results presented in reference 4 and were held constant when the slat angle, defined in figure 3, was varied.

As shown in figures 1 and 3, the trailing-edge flap employed for the investigation had a 0.25c' chord, a span of 0.469b/2, and a deflection angle of 45° measured normal to the 0.50c' line.

Flush surface static-pressure orifices were installed in the slat in three chordwise rows in the stream direction and in the wing in two chordwise rows in the stream direction and seven chordwise rows normal to the 0.50c' line. The general spanwise arrangement of these pressure orifices is shown in figure 4 and their chordwise locations are presented in table I.

TESTS AND CORRECTIONS

Both force and pressure measurements were obtained during the investigation. The force-data phase of the program was conducted over an angle-of-attack range from approximately -2° to 31°. The slat parameters varied during the test program were the slat deflection angle (with the slat span held constant at 1.00b/2) and the slat span (for a slat deflection angle of 45°). For the two test configurations, the basic wing and the wing with the 0.50b/2 span slat deflected 45°, the test Reynolds number was varied from 2.9×10^6 to 6.1×10^6. The remainder of the test program was conducted only at a Reynolds number of 6.1×10^6 and a Mach number of 0.10.

Chordwise pressure distributions and tuft surveys were obtained at four representative angles of attack for the following conditions: (a) basic wing, (b) wing with 0.50b/2 span slat deflected 45°, and (c) configuration (b) with the trailing-edge flap deflected.

The jet-boundary corrections applied to the force data, as discussed in reference 3, presented herein were based on the method presented in reference 5 and were added to the uncorrected results.

$$\Delta\alpha = -0.84C_L$$

$$\Delta C_D = -0.01281C_L^2$$

$$\Delta C_m = -0.00427C_L$$

The data have also been corrected for the effects of blockage and stream angle.

RESULTS AND DISCUSSION

The results of the force tests are presented in figures 5 to 8, the wing flow surveys in figure 9, the pressure distributions over the wing in figures 10 through 13, and the chordwise pressure distributions and loads on the slat in figures 14 to 16.

Aerodynamic Characteristics

Basic wing.- The effects of Reynolds number on the aerodynamic characteristics of the basic wing are presented in figure 5. The data exhibit the trends characteristic of the results obtained for a thin sweptback wing having the leading-edge separation vortex type of flow. The lift coefficient at which the increase in wing lift-curve slope (which is inherent with the separation-vortex type of flow) initially occurs increases in magnitude with Reynolds number (fig. 5(a)). The lift-curve slope measured through zero lift agrees with the value predicted by using the Weissinger method (reference 6). The $C_{L_{max}}$ obtained at $R = 6.1 \times 10^6$ was approximately 1.00, or about 0.02 higher than the $C_{L_{max}}$ reached for a test Reynolds number of 2.9×10^6.

The increased tendency for the experimental drag curve to depart from the theoretical drag curve $C_{D_o} + \frac{C_L^2}{\pi A}$ in the low-lift range with a decrease in Reynolds number shows the unfavorable influence that decreasing R exerts on the flow characteristics of the wing (fig. 5(b)). A comparison of the drag data, on the basis of constant lift coefficient, indicates that C_D is decreased by an increase in the test Reynolds number throughout the lift range above about $C_L = 0.3$.

Varying the Reynolds number over the range investigated does not appear to alter significantly the general shape of the pitching-moment and spanwise-center-of-pressure curves (figs. 5(c) and 5(d)).

Effect of slat deflection angle.- The effect of the slat deflection angle δ_s was determined only for the full-span slat arrangement (fig. 6). An increase in $C_{L_{max}}$ is obtained by increasing δ_s up to the highest slat deflection angle tested (fig. 6(a)). At $\delta_s = 45^\circ$, $C_{L_{max}}$ is approximately 1.17 as compared to about 1.00 for the basic wing.

The improvement in the drag characteristics of the wing obtained by increasing the slat deflection may be illustrated by the fact that, at a lift coefficient of 1.00, the drag of the wing with the full-span slat deflected 20° is approximately 80 percent greater than that measured for the $\delta_s = 45^\circ$ configuration.

Deflection of the full-span slat results in instability of the wing over the entire lift range from zero lift to maximum lift (fig. 6(c)). Up to a moderately high lift coefficient the wing with the slat deflected is moderately unstable and then, very abruptly, becomes highly unstable. The abrupt change in stability, similar to the characteristics obtained

with the basic wing, is caused by a loss of lift outboard, as indicated by the inboard movement of the spanwise center of pressure in figure 6(d) and by the decrease in the wing lift-curve slope in the same lift-coefficient range where this stability change occurs (fig. 6(a)). Increasing δ_s increases the magnitude of the C_L at which the abrupt change in stability occurs (fig. 6(c)). For the wing with the full-span slat deflected 45°, the change in stability from the moderate to the high lift range is approximately equivalent to a $0.4\bar{c}$ shift forward of the wing center of pressure. As in the case of the basic wing, a stable change in the pitching-moment characteristics is obtained at the stall for all of the deflected full-span slat configurations tested.

Effect of slat span.- Figure 7 illustrates the influence of the span of the extended slat, $\delta_s = 45°$, on the aerodynamic characteristics of the wing. Increasing the slat span has no effect on $C_{L_{max}}$ for spans shorter than 0.625b/2 but produces significant increases in $C_{L_{max}}$ for spans between 0.75b/2 and 1.00b/2.

As shown in figure 7(b), correspondingly greater decreases in drag are obtained in the moderate and high-lift range as compared to the characteristics of the basic wing as successively longer slat spans than 0.25b/2 are employed.

The general trend of the longitudinal stability and spanwise center of pressure with lift coefficient (figs. 7(c) and 7(d), respectively) indicates a stability change for slat spans greater than 0.50b/2. For slat spans of 0.75b/2 and 1.00b/2 (fig. 7(d)), the location of the spanwise center of pressure remains fairly constant over a large range of lift coefficients. Between C_L of 0.2 and 0.5, however, the length of slat span does not appear to alter the spanwise location of the center of pressure (fig. 7(d)) and the difference in stability in the low-lift range, shown in figure 7(c), is probably caused by a more forward chordwise shift of the center of pressure due to the use of the longer slat spans. For both the basic wing and the configurations of slat spans greater than 0.50b/2, the wing becomes highly stable at $C_{L_{max}}$, whereas for the shorter slat spans, 0.25b/2 and 0.375b/2, this stable effect occurs initially at a C_L about 0.1 lower than $C_{L_{max}}$. This effect may be correlated with the variations in spanwise location of the wing center of pressure near $C_{L_{max}}$ (fig. 7(d)).

0.50b/2 slat span.- On the basis of the stability characteristics shown in figure 7(c), the $0.50\frac{b}{2}$-slat configuration was selected as the optimum arrangement of those investigated, to use for the pressure-distribution tests. The effect of Reynolds number on this configuration

is presented in figure 8. Over the Reynolds number range investigated, there is little or no change in the lift and drag characteristics with a variation in Reynolds number (figs. 8(a) and 8(b)).

The pitching characteristics, (fig. 8(c)) for the three highest Reynolds number tests are closely comparable and differ from the results obtained at $R = 2.9 \times 10^6$ in that the instability exhibited in the moderate lift range begins at a lower C_L for $R = 2.9 \times 10^6$.

Wing Flow Characteristics

Tuft surveys.- The stalling characteristics of the wing as determined from the tuft studies are presented in figure 9. Extension of the slat caused rough flow in the area behind the inboard end of the slat at moderate lift coefficients. With increased lift, the region of disturbed flow increased both inboard and outboard. The slat, however, improved the stalling characteristics of the tip section and, immediately behind the wing-slat gap, the flow remained smooth and alined normal to the leading edge of the wing up to high lift coefficients.

Pressure distributions.- Representative chordwise pressure distributions are presented in figures 10 to 12 and the notation used therein for identifying the measuring stations corresponds to the layout sketch shown in figure 4. It should be noted that stations H and J are located streamwise, whereas stations C, D, E, and F are alined normal to the 0.50c' line.

In order to provide a more graphic representation of the over-all flow characteristics of the wing, upper-wing surface-pressure isobars (lines of constant pressure) have been presented in figure 13. In addition to the data shown in figures 10 to 12, the data obtained at wing stations A, B, and G (fig. 4) were also used in determining the isobar plots. In instances where the shape of the contour is in doubt, due to an insufficient number of data points, the isobar lines have been dashed. In all these cases, however, the contouring has been based on a consideration of the following: the shape of the adjoining experimentally determined isobars; approximate P values derived from limited extensions of the faired chordwise pressure-distribution curves; and the results of previous pressure investigations on wings having similar flow characteristics (such as references 3 and 7).

The chordwise pressure distributions (fig. 10) are characteristic of the type usually obtained with a leading-edge separation vortex and agree, qualitatively, with the pressure measurements presented in reference 7 for a sharp-nose wing having approximately the same plan form as the subject wing. The relative chordwise location of the vortex

core at any particular station is indicated by the "hump" or local increase in the upper surface pressure. (See, for example, section F in figure 10(b) and sections C, D, and E in figure 10(c).) Over the rear of the airfoil section, just behind the vortex core, there is a severe loss in suction pressure. The data of reference 3 indicate that this loss of lift over the rear of the airfoil is regained, however, when the section stalls and results in a large rearward shift in the chordwise center of pressure, as much as 0.20c for the wing of reference 3.

It is of interest to note the large leading-edge negative pressure peaks obtained at station H. It would appear that the boundary-layer drainage near the wing root, induced by the spanwise flow characteristics of the wing, allows the inboard wing sections to operate at very high angles of attack without stalling.

With the 0.50b/2 slat deflected (figs. 11 and 12), the presence of a separation vortex is indicated in the pressure distributions for the stations inboard of the slat but not at the outboard chordwise stations located behind the slat. This result agrees with the flow observations discussed in reference 8 for which, with a leading-edge flap deflected, it was noted that the leading-edge separation vortex turned into the stream direction and trailed off the wing at a point just inboard of the inboard end of the leading-edge flap.

At the higher angles of attack, the pressure distributions at the chordwise stations immediately behind the slat confirm the indications of the tuft surveys (fig. 9), which showed the flow in this region to be unstalled. This result is in direct contrast to the severe outboard stall obtained with the basic wing.

The contoured suction pressure plots of figure 13 illustrate the progression of the wing stall with increasing lift for the basic wing. At a $C_L = 0.435$, the isobars are directed toward the wing tip. With an increase in lift to $C_L = 0.712$, there is a distinct flow change and the isobars appear to be severely swept back with the outboard part of the isobars first turning in a streamwise direction toward the leading edge of the wing and then turning again in a spanwise direction. The part of the isobar between the two bends correlates with the chordwise pressure distributions as being the approximate chordwise location of the separation vortex. Thus, two lines drawn from the wing apex through these two sets of bends in the isobars would seem to locate, roughly, the position of the separation vortex on the wing at this lift coefficient, 0.712. Because of the more rearward position of the outboard portion of the vortex and since the chordwise extent of the pressure tubes ends at approximately 0.60c', it is more difficult to locate the boundary of the vortex from the isobar diagrams at the higher lift coefficients.

With the 0.50b/2 slat deflected, the isobar contours graphically illustrate the growth of the stalled region just inboard of the inboard end of the slat (figs. 13(b) and 13(c)). The tuft surveys and pressure isobars agree qualitatively in illustrating that, as $C_{L_{max}}$ is approached, the general stalling pattern obtained on the wing with the 0.50b/2 slat deflected does not appear to be altered by deflection of the trailing-edge flap. (Compare figs. 9(b) and 13(b) with figs. 9(c) and 13(c), respectively.)

Slat Load Characteristics

The chordwise pressure distributions over the 0.50b/2 slat are shown in figures 14 and 15 for the wing with the slat deflected alone and in combination with the trailing-edge flap. The lower station on figures 14 and 15 represents the inboard station (fig. 4). It should be noted that the lower-surface orifice tube at $0.20c_s$, which generally indicates a negative pressure, is located in the severest part of the discontinuity in the lower surface of the slat (fig. 3).

The location of the chordwise center of pressure of the slat load and the slat normal-force coefficient were determined from the slat pressure distribution only for the middle chordwise station on the slat (fig. 4). It is believed that the pressure measurements at this station are more representative of the over-all slat loads than are the pressure data at the stations near the ends of the slat which were probably affected by end-flow conditions.

The variation of the slat chordwise center of pressure with lift coefficient, presented in figure 16, does not appear to be affected by the deflection of the trailing-edge flap. As C_L is increased from the lowest value at which pressure data were obtained, the slat chordwise center of pressure moves slightly forward but then shifts rapidly rearward at the lift coefficient corresponding to wing stall.

The normal force on the slat increases sharply in magnitude with increasing lift coefficient (fig. 16) in the lift range investigated and attains its maximum value when the wing is operating, approximately, at maximum lift. Below the lift coefficient corresponding to $C_{L_{max}}$ for the wing with the 0.50b/2 slat deflected alone, c_{n_s} is decreased when the trailing-edge flap is deflected.

CONCLUSIONS

An investigation has been conducted of a 15-percent-chord slat installed on a 49.1° sweptback wing having an aspect ratio of 3.78 and incorporating NACA 65A006 airfoil sections streamwise. The results indicate that for the subject wing configuration:

1. On the basis of static longitudinal stability, a slat span of 0.50b/2 is the most effective of the slat spans investigated.

2. Slat spans shorter than 0.625b/2 produced no increase in maximum lift.

3. At a given lift coefficient, increasing the slat span and/or the slat deflection, up to 45°, reduced the drag characteristics of the wing in the moderate and high lift range.

4. Deflecting a trailing-edge flap had little effect on the chordwise location of the slat-load center of pressure.

5. At a given lift coefficient below the value corresponding to $C_{L_{max}}$ for the wing with the 0.50b/2 slat deflected alone, the slat normal force is decreased when the trailing-edge flap is deflected.

Langley Aeronautical Laboratory
National Advisory Committee for Aeronautics
Langley Field, Va.

REFERENCES

1. Graham, Robert R., and Conner, D. William: Investigation of High-Lift and Stall-Control Devices on an NACA 64-Series 42° Sweptback Wing with and without Fuselage. NACA RM L7G09, 1947.

2. Koven, William, and Graham, Robert R.: Wind-Tunnel Investigation of High-Lift and Stall-Control Devices on a 37° Sweptback Wing of Aspect Ratio 6 at High Reynolds Numbers. NACA RM L8D29, 1948.

3. Lipson, Stanley, and Barnett, U. Reed, Jr.: Comparison of Semispan and Full-Span Tests of a 47.5° Sweptback Wing with Symmetrical Circular-Arc Sections and Having Drooped-Nose Flaps, Trailing-Edge Flaps, and Ailerons. NACA RM L51H15, 1951.

4. Gottlieb, Stanley M.: Two-Dimensional Wind-Tunnel Investigation of Two NACA 6-Series Airfoils with Leading-Edge Slats. NACA RM L8K22, 1949.

5. Sivells, James C., and Salmi, Rachel M.: Jet-Boundary Corrections for Complete and Semispan Swept Wings in Closed Circular Wind Tunnels. NACA TN 2454, 1951.

6. DeYoung, John: Theoretical Additional Span Loading Characteristics of Wings with Arbitrary Sweep, Aspect Ratio, and Taper Ratio. NACA TN 1491, 1947.

7. Lange, Roy H., Whittle, Edward F., Jr., and Fink, Marvin P.: Investigation at Large Scale of the Pressure Distribution and Flow Phenomena over a Wing with the Leading Edge Swept Back 47.5° Having Circular-Arc Airfoil Sections and Equipped with Drooped-Nose and Plain Flaps. NACA RM L9G15, 1949.

8. Salmi, Reino J.: Effects of Leading-Edge Devices and Trailing-Edge Flaps on Longitudinal Characteristics of Two 47.7° Sweptback Wings of Aspect Ratio 5.1 and 6.0 at a Reynolds Number of 6.0×10^6. NACA RM L50F20, 1950.

TABLE I.- CHORDWISE LOCATION OF ORIFICE TUBES

[Station letters and numbers refer to spanwise locations given in fig. 4]

Station A

Upper surface (Percent c')	Lower surface (Percent c')
0.0	5.0
.10	10.0
.25	25.0
1.0	51.0
2.0	
5.0	
10.0	
20.0	
41.0	
60.0	

Stations B, C, D

Upper surface (Percent c')	Lower surface (Percent c')
0.0	5.0
.10	10.0
.25	25.0
1.0	51.0
2.0	
5.0	
10.0	
18.0	
41.0	
58.0	

Stations E, F, G

Upper surface (Percent c')	Lower surface (Percent c')
0.0	5.0
.10	10.0
.25	25.0
1.0	51.0
2.0	
5.0	
10.0	
18.0	
40.0	
58.0	

Station H

Upper surface (Percent c)	Lower surface (Percent c)
0.0	5.0
.10	10.0
.25	25.0
1.0	50.0
2.0	
5.0	
10.0	
20.0	
45.0	
60.0	

Station J

Upper surface (Percent c)	Lower surface (Percent c)
0.0	5.0
.10	10.0
.25	25.0
1.0	
2.0	
5.0	
10.0	
29.0	
50.0	

Stations 1 and 2

Upper surface (Percent c'_s)	Lower surface (Percent c'_s)
0.0	5.0
2.0	20.0
5.0	50.0
10.0	
30.0	
50.0	

Station 3

Upper surface (Percent c'_s)	Lower surface (Percent c'_s)
0.0	2.0
2.0	5.0
5.0	10.0
10.0	20.0
30.0	30.0
50.0	50.0

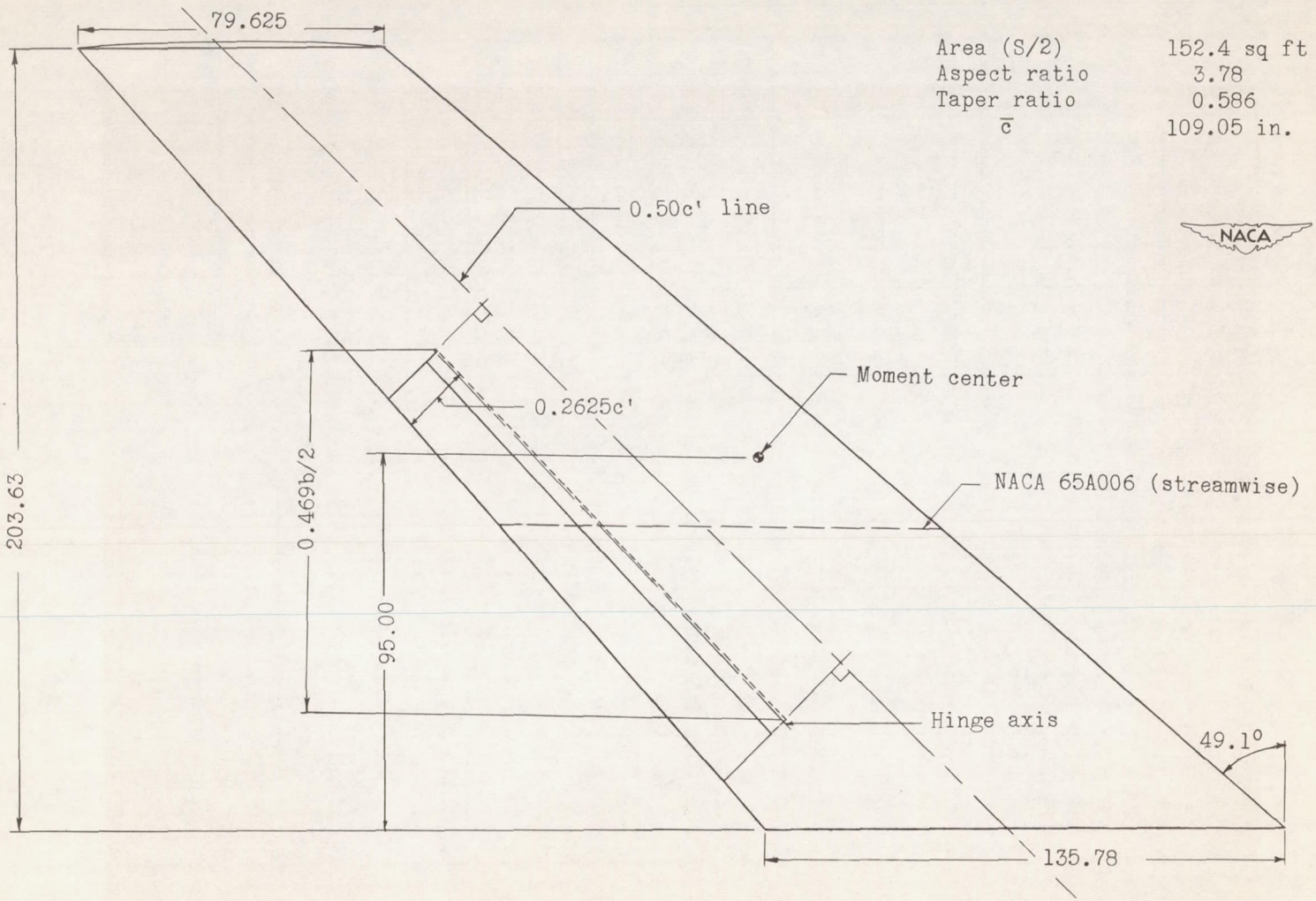


Figure 1.- Plan form of semispan 49.1° sweptback wing. All dimensions are in inches.

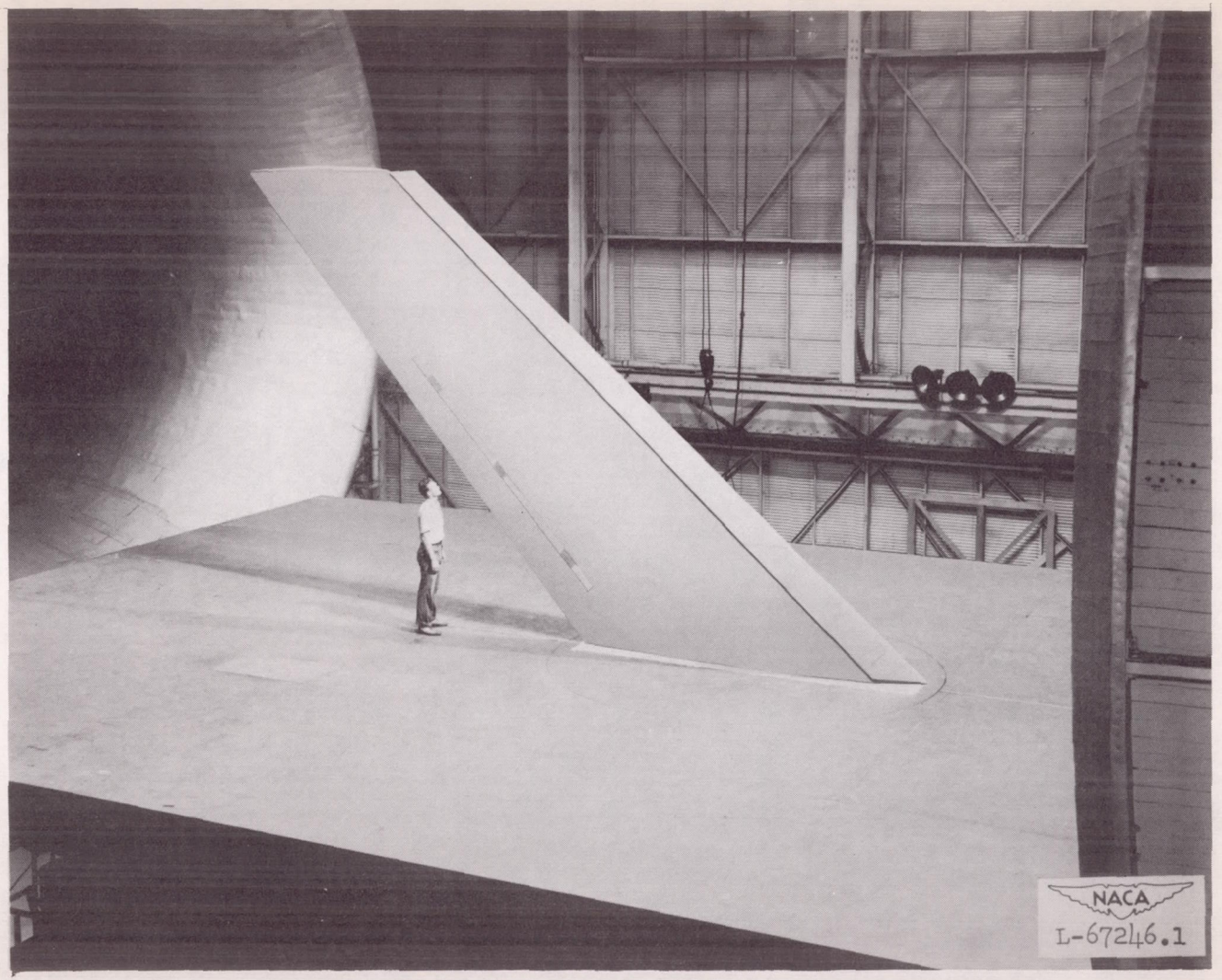
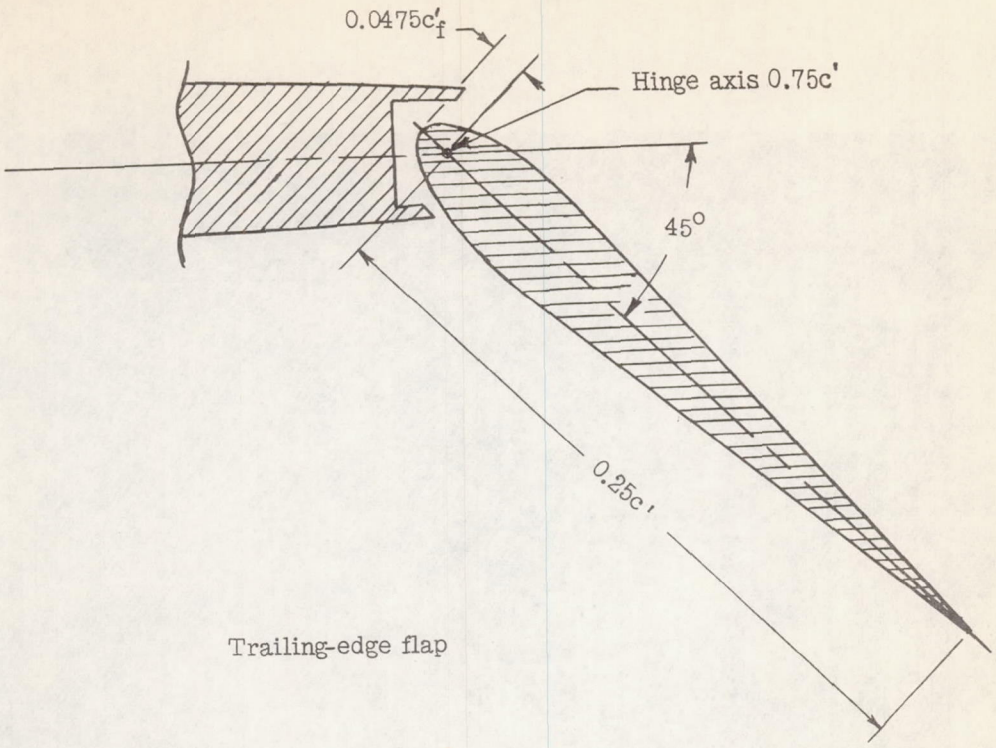
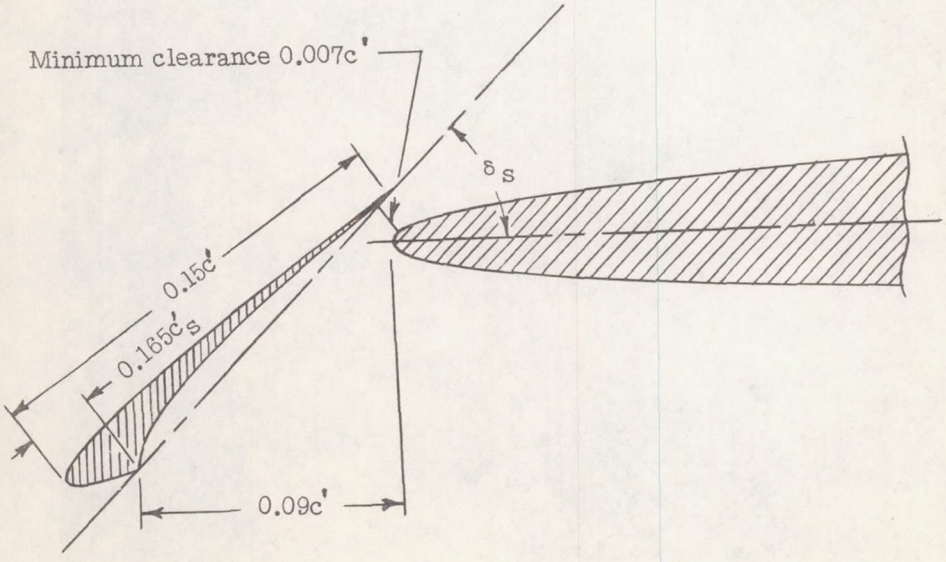


Figure 2.- The semispan 49.1° sweptback wing, with full-span slat installed, mounted in the Langley full-scale tunnel.



Trailing-edge flap



Leading-edge slat

Figure 3.- Leading-edge slat and trailing-edge flap as installed on semispan 49.1° sweptback wing. All views taken normal to 0.50c' line.

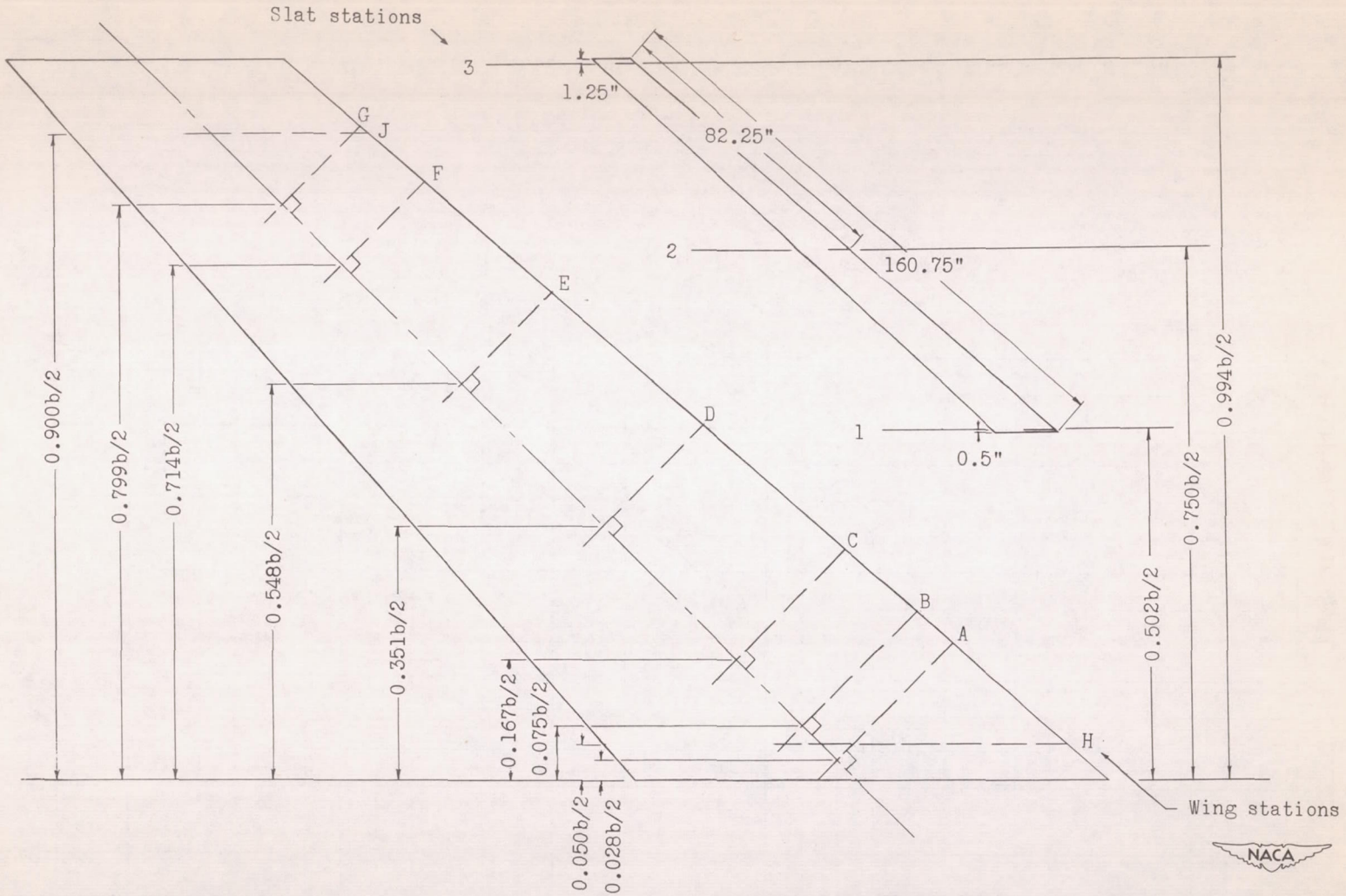
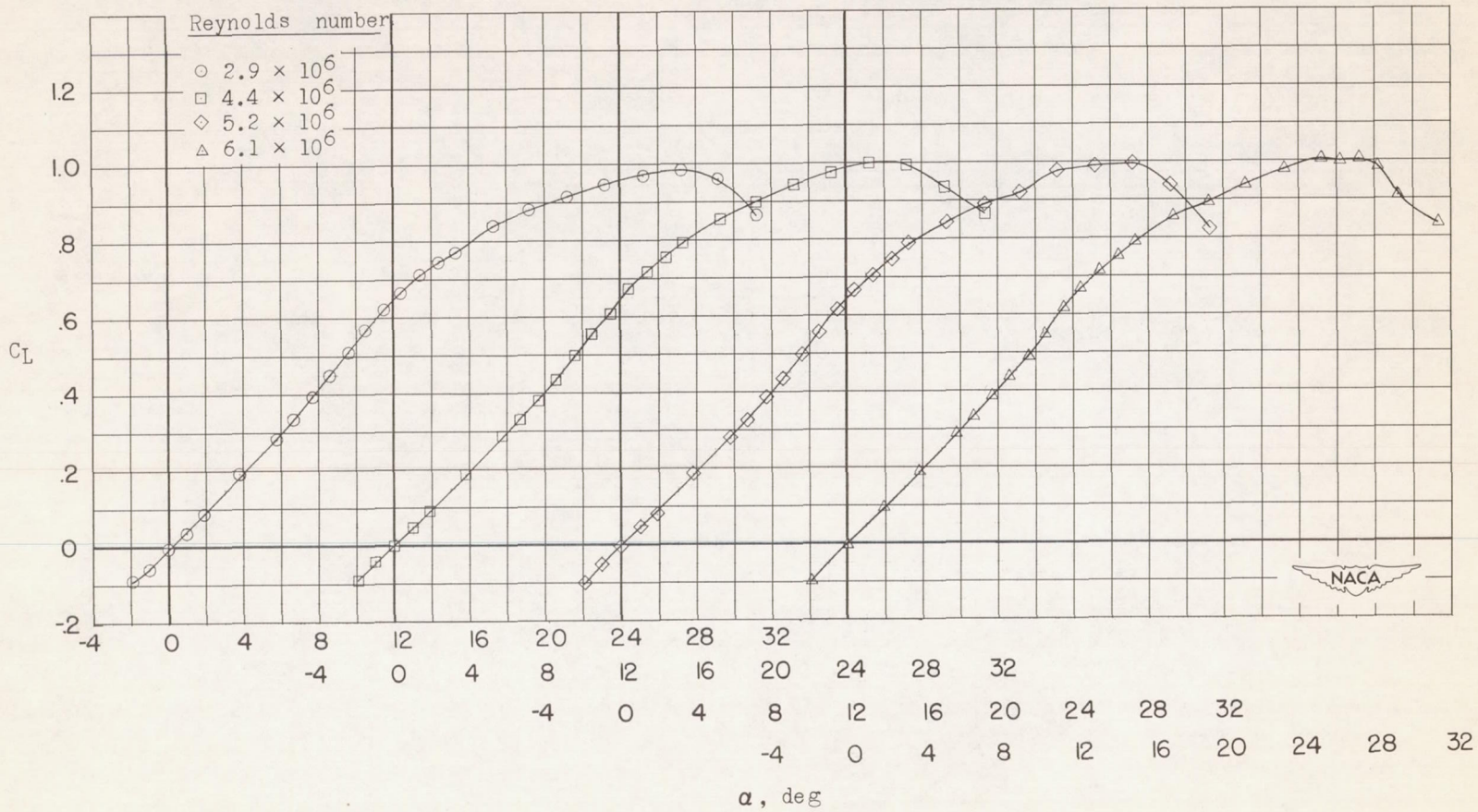
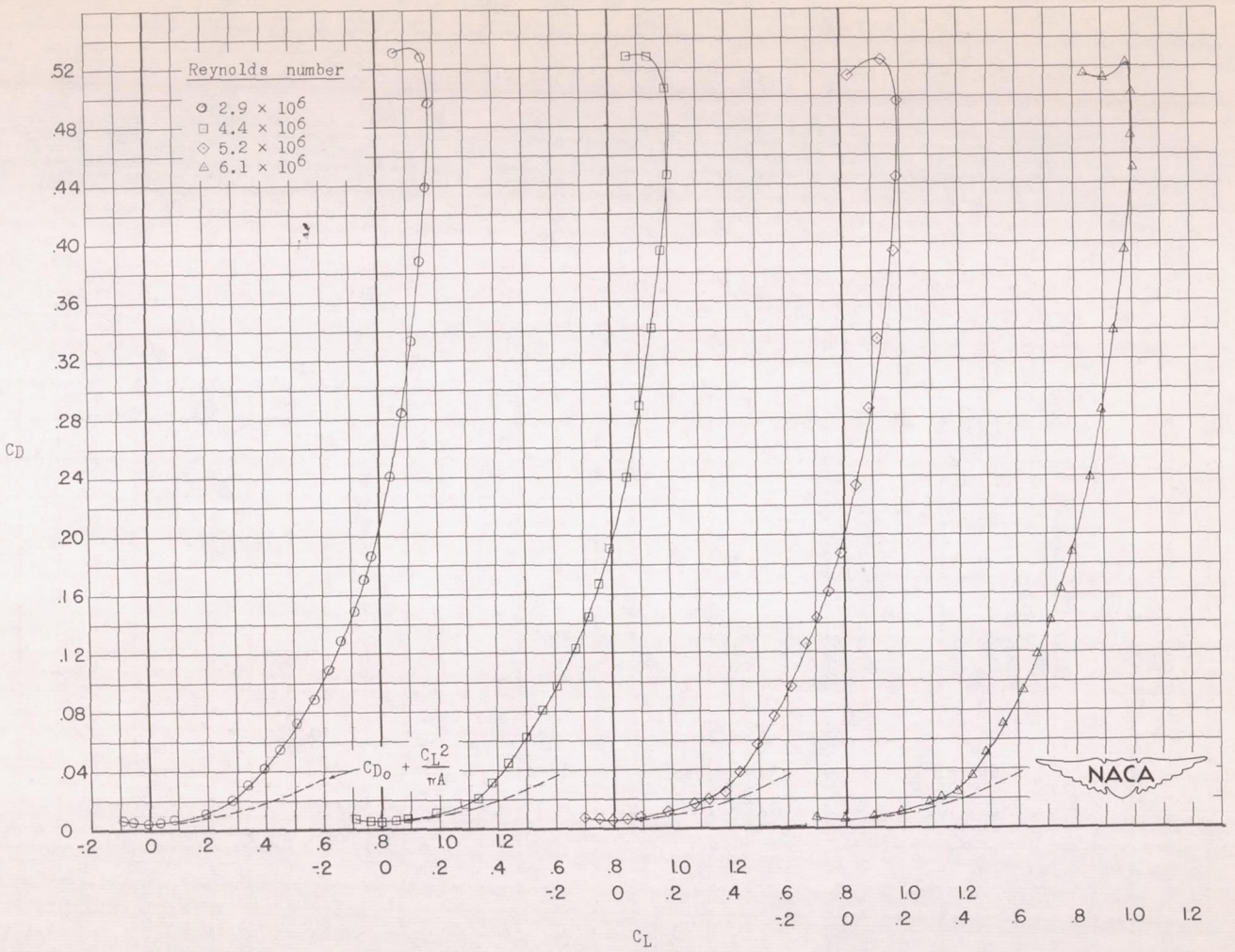


Figure 4.- Spanwise location of pressure measuring stations on semispan 49.1° sweptback wing and slat.



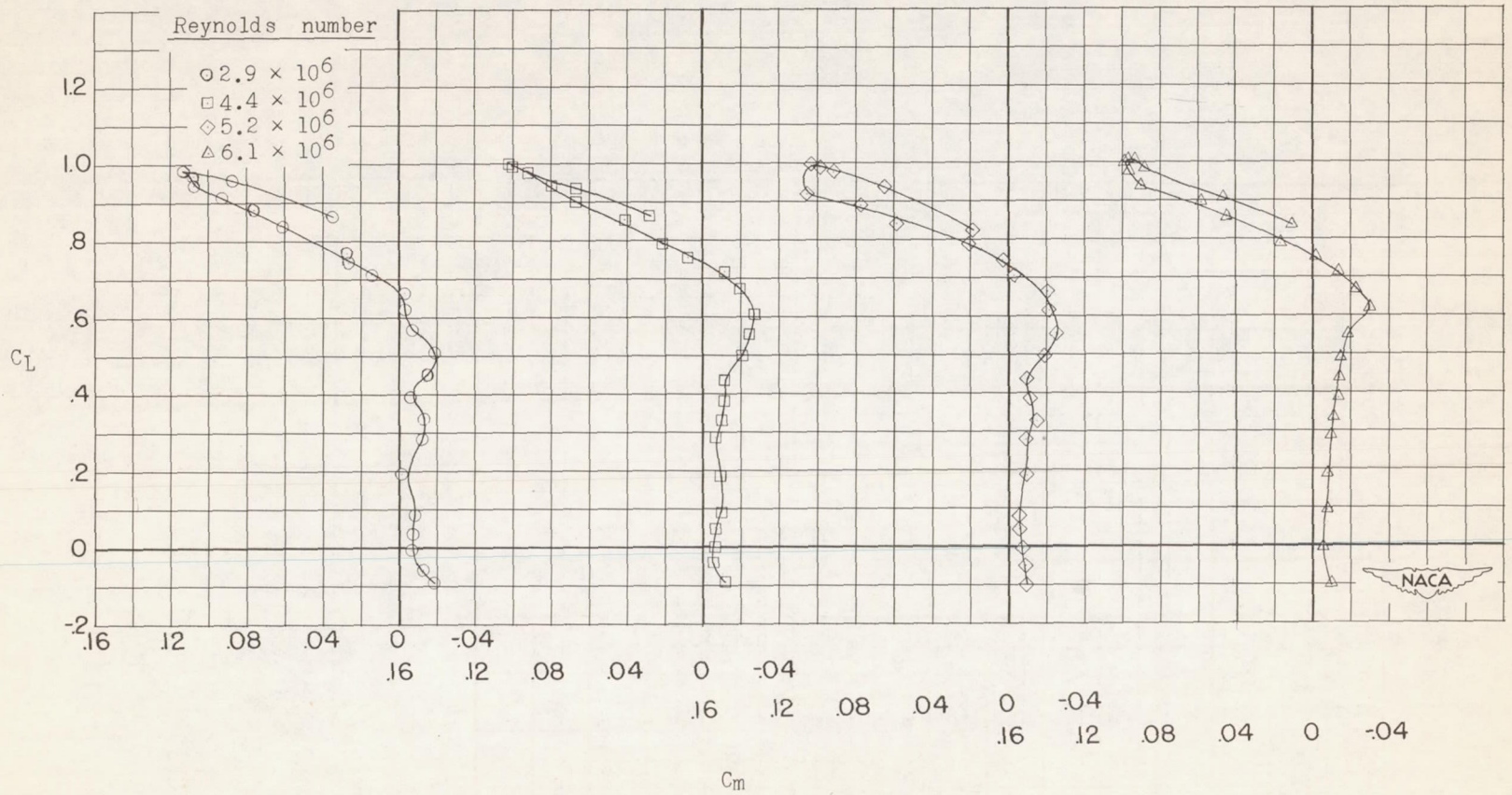
(a) C_L against α.

Figure 5.- Effect of Reynolds number on the aerodynamic characteristics of the semispan 49.1° sweptback wing; basic wing.



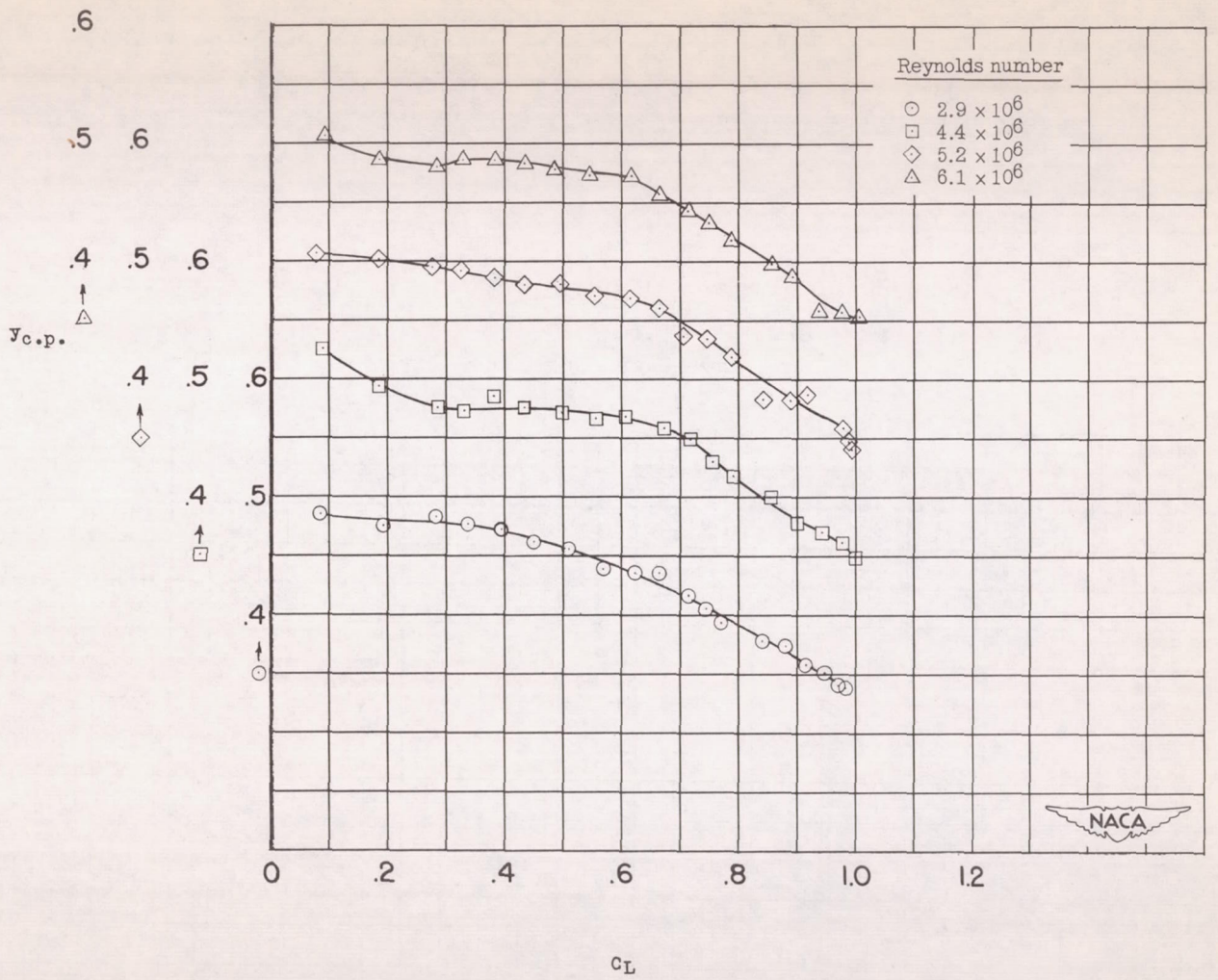
(b) C_D against C_L.

Figure 5.- Continued.



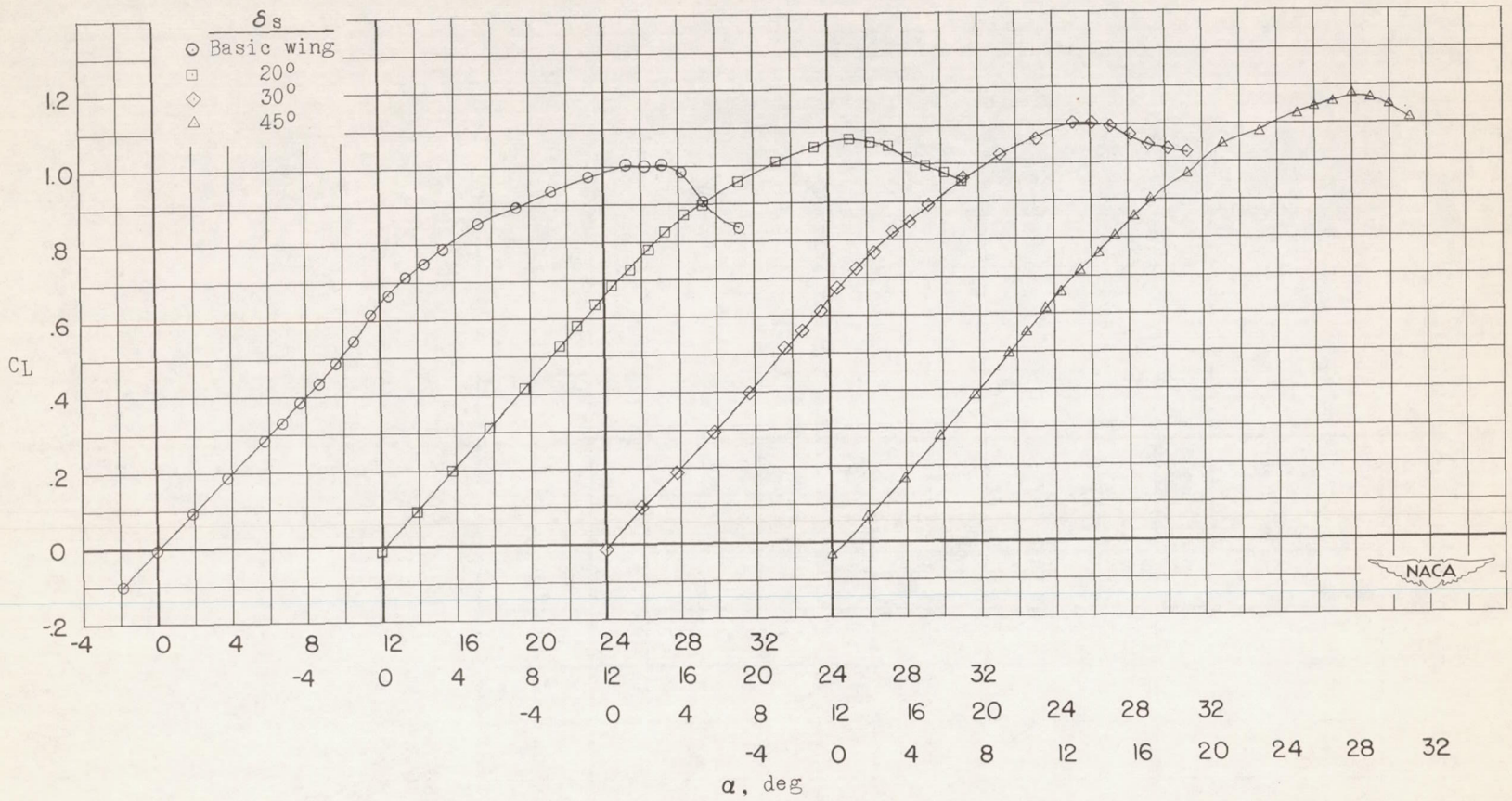
(c) C_m against C_L.

Figure 5.- Continued.



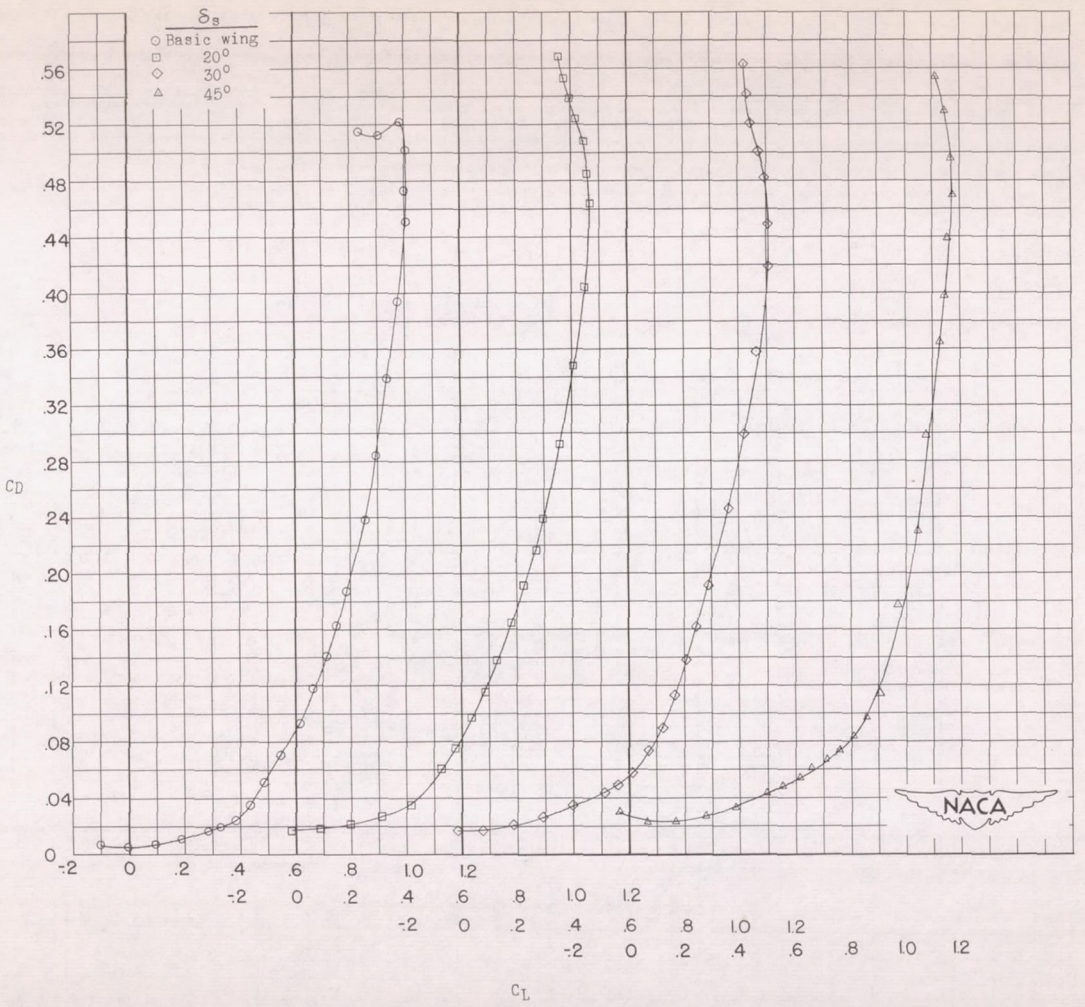
(d) $y_{c.p.}$ against C_L.

Figure 5.- Concluded.



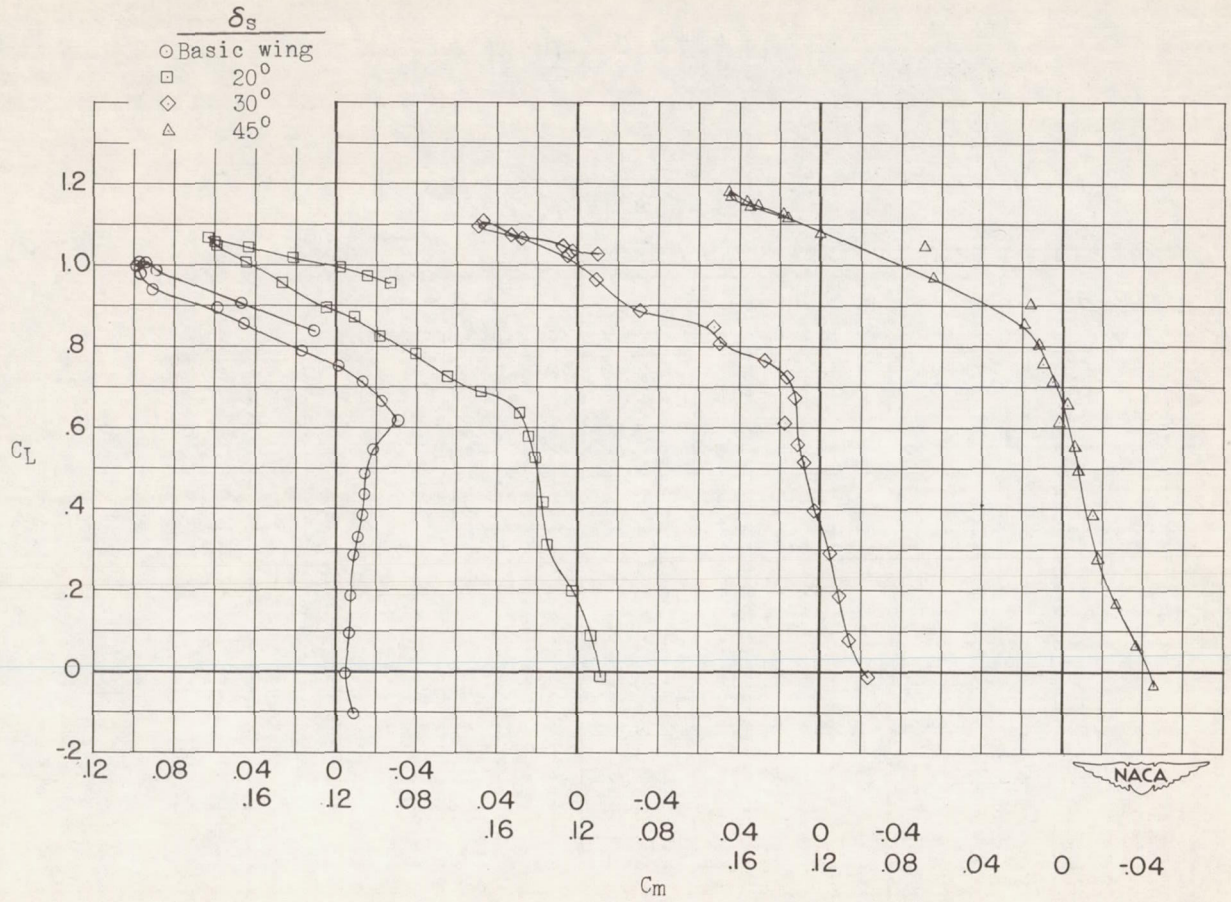
(a) C_L against α.

Figure 6.- Effect of slat deflection angle on the aerodynamic characteristics of the semispan 49.1° sweptback wing. Full-span slat installed; $R = 6.1 \times 10^6$.



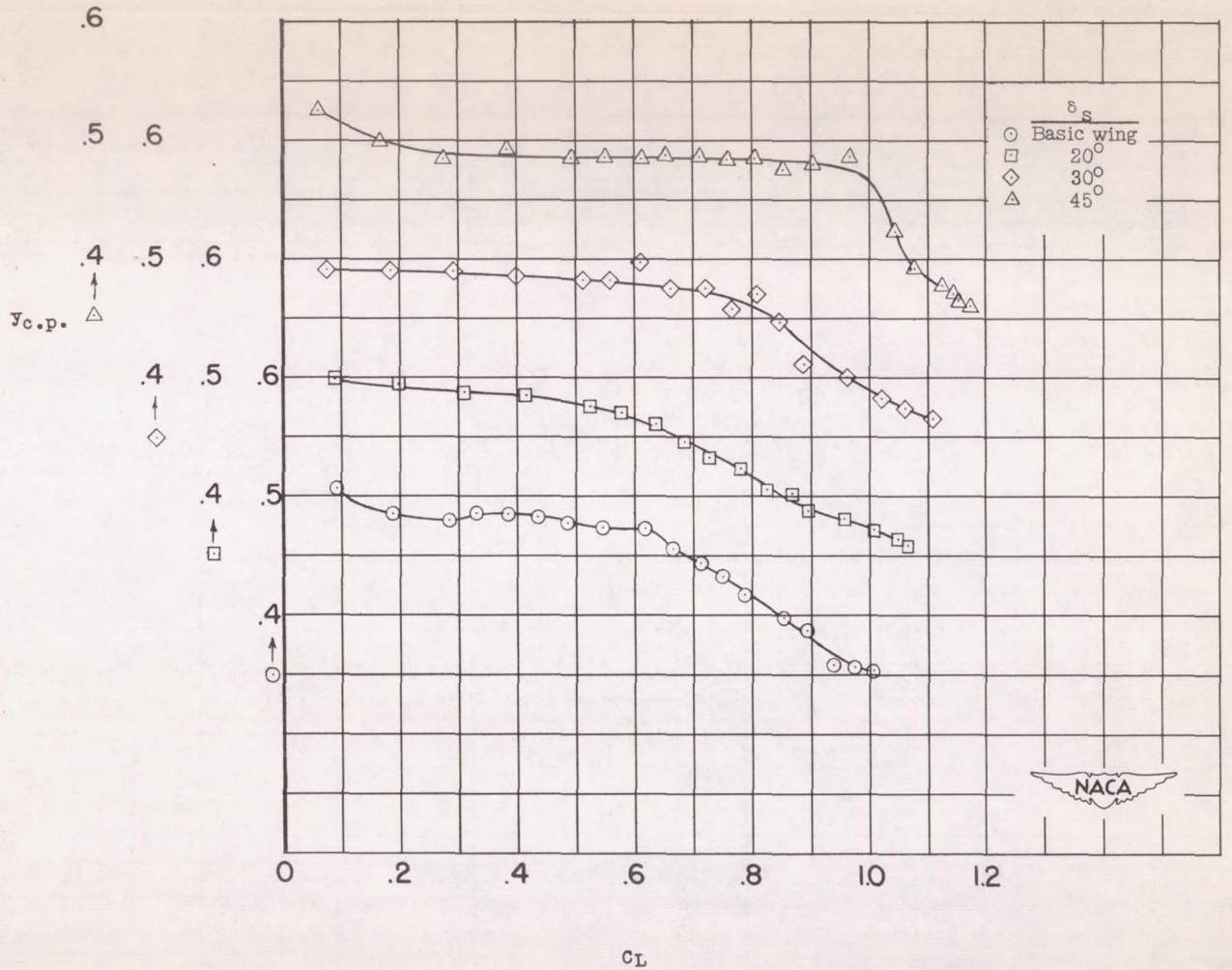
(b) C_D against C_L.

Figure 6.- Continued.



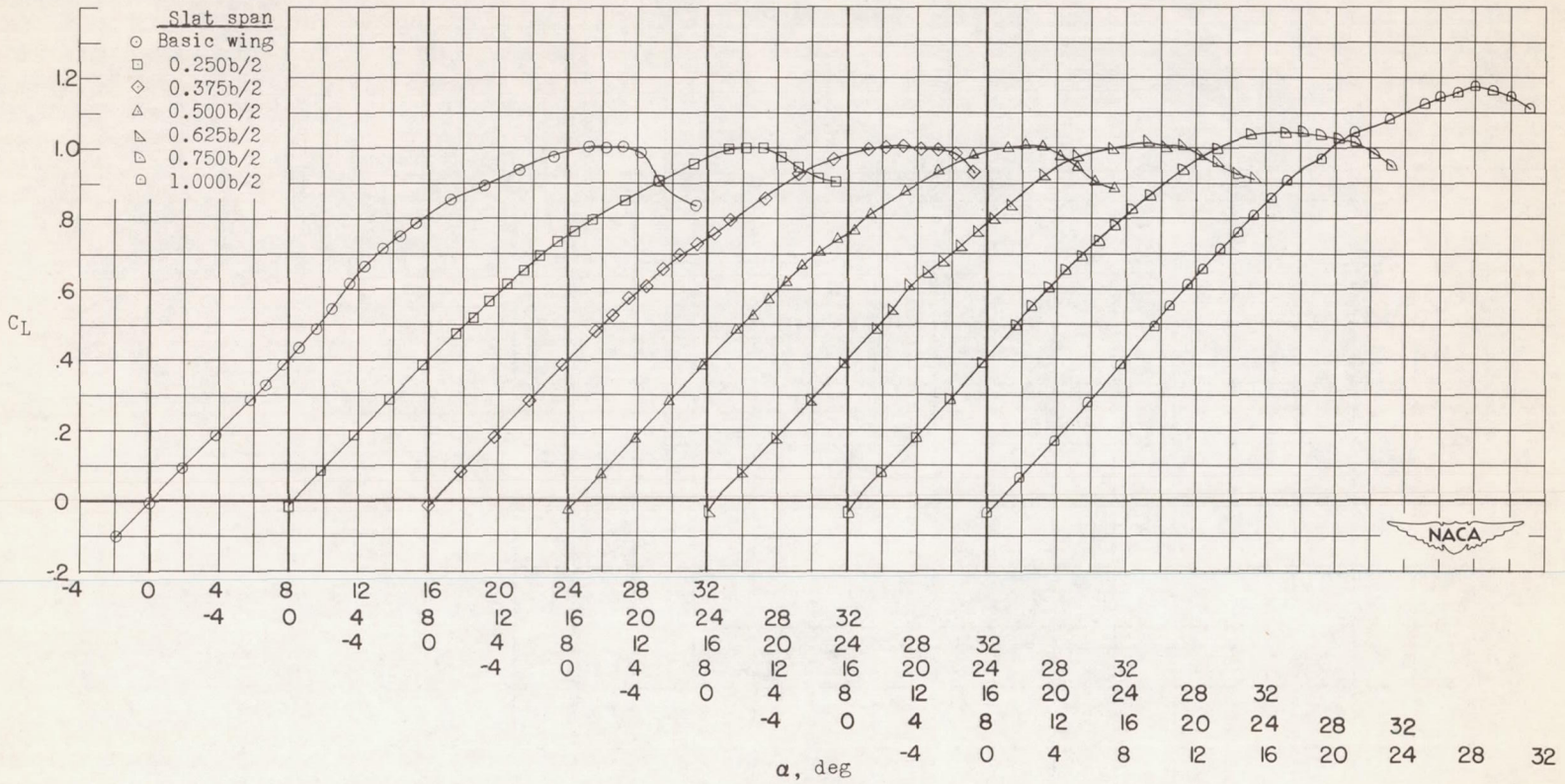
(c) C_m against C_L.

Figure 6.- Continued.



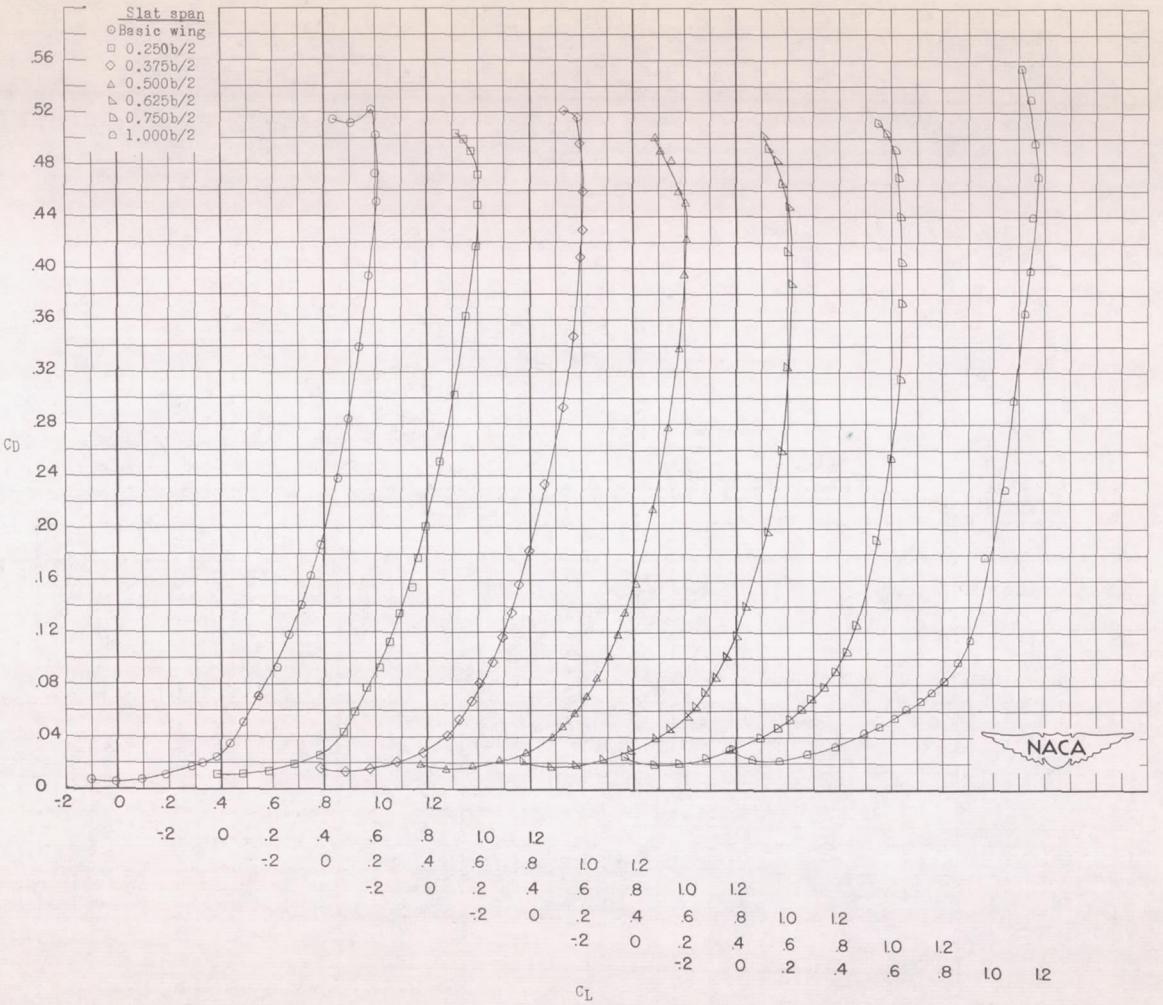
(d) $y_{c.p.}$ against C_L.

Figure 6.- Concluded.



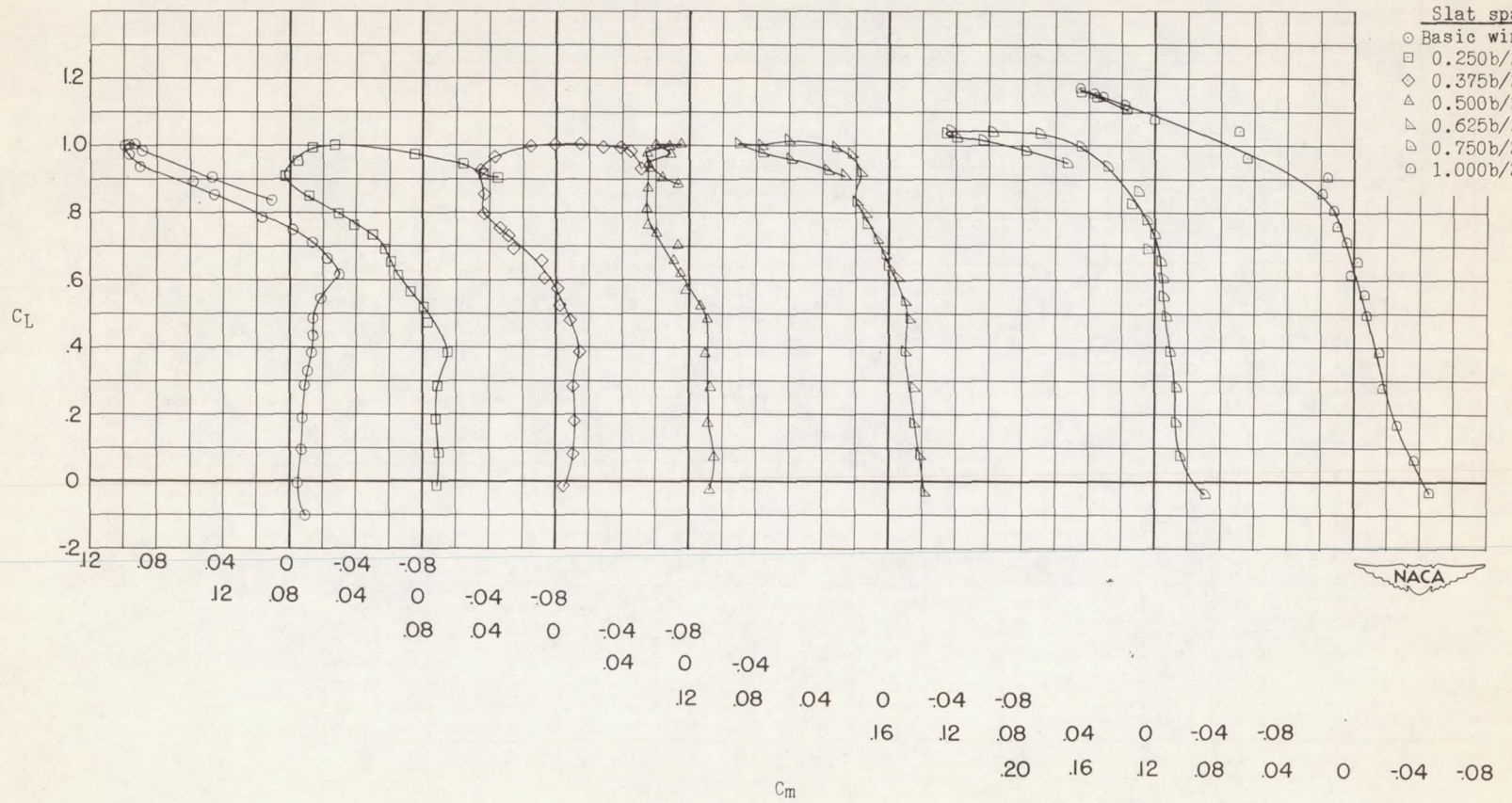
(a) C_L against α.

Figure 7.- Effect of slat span on the aerodynamic characteristics of the semispan 49.1° sweptback wing. $\delta_s = 45°$; $R = 6.1 \times 10^6$.



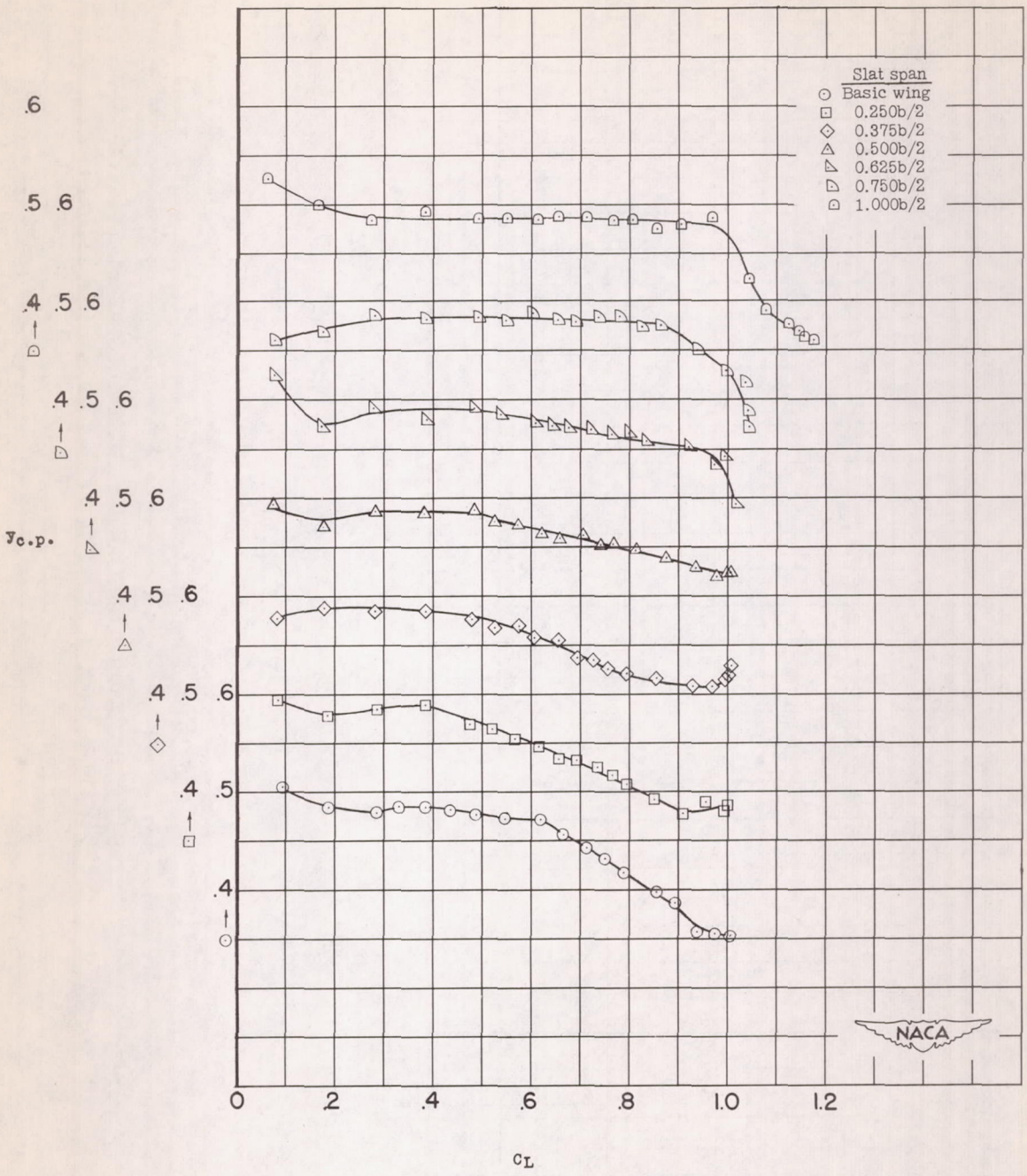
(b) C_D against C_L.

Figure 7.- Continued.



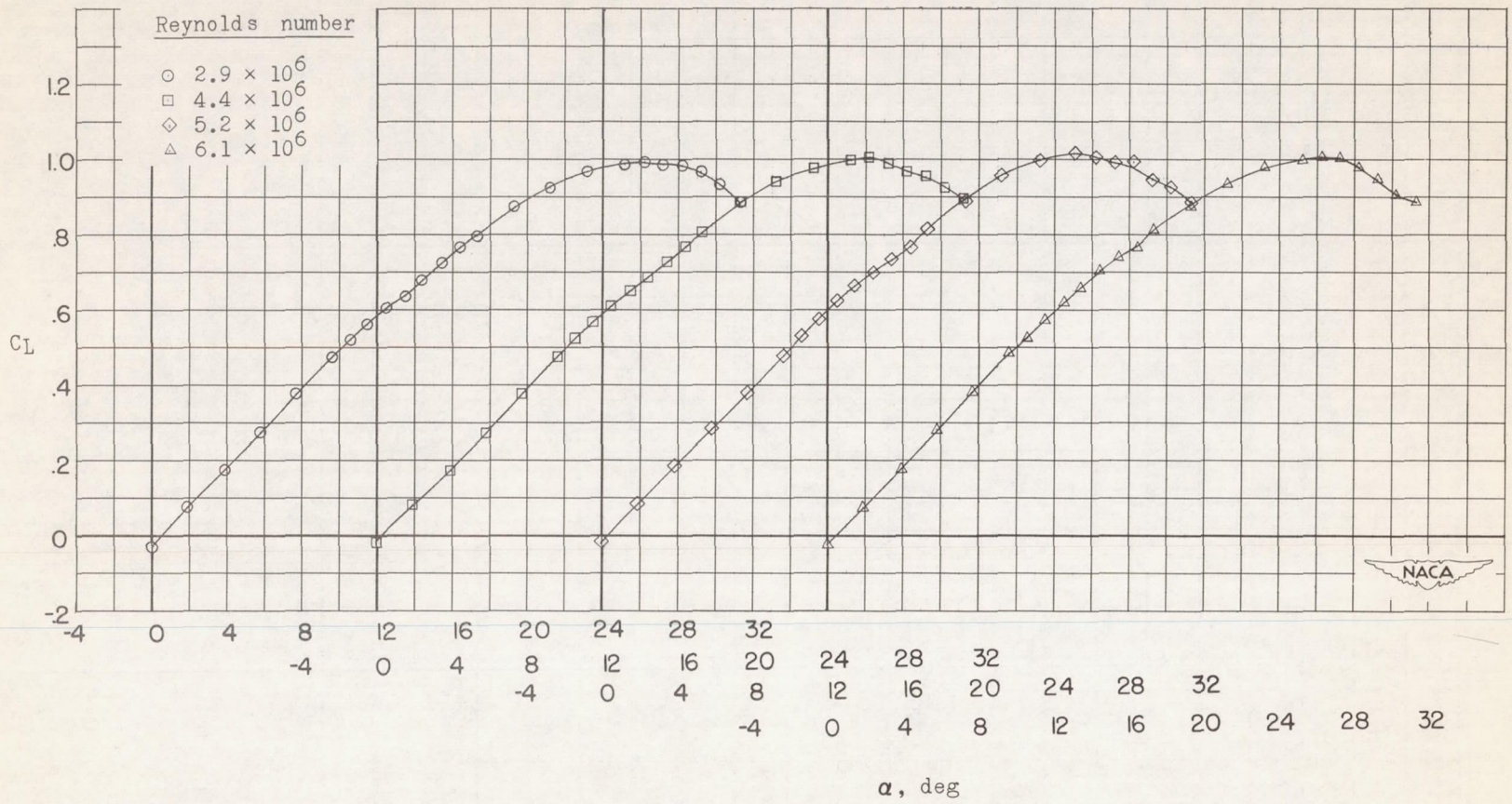
(c) C_m against C_L.

Figure 7.- Continued.



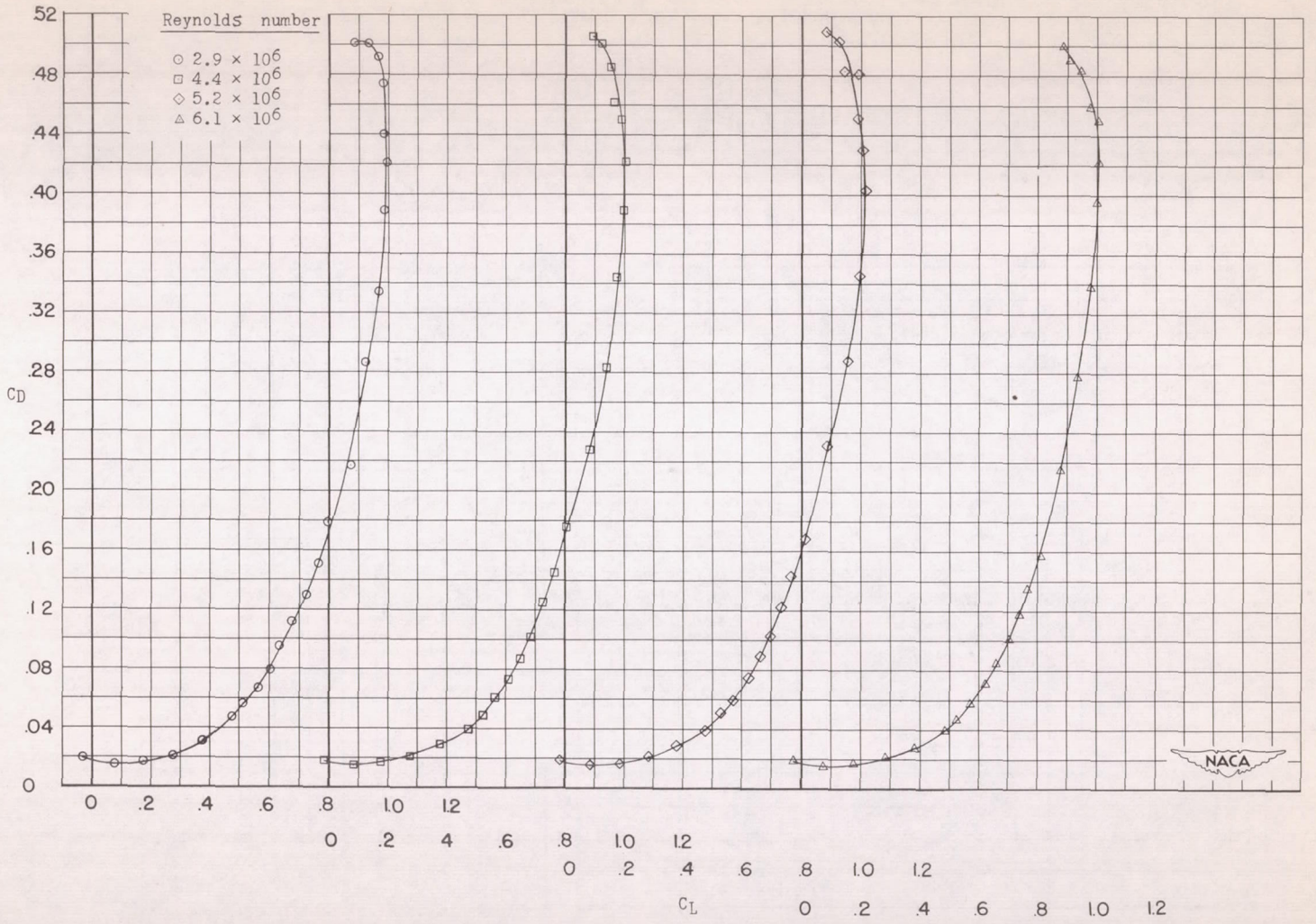
(d) $y_{c.p.}$ against C_L.

Figure 7.- Concluded.



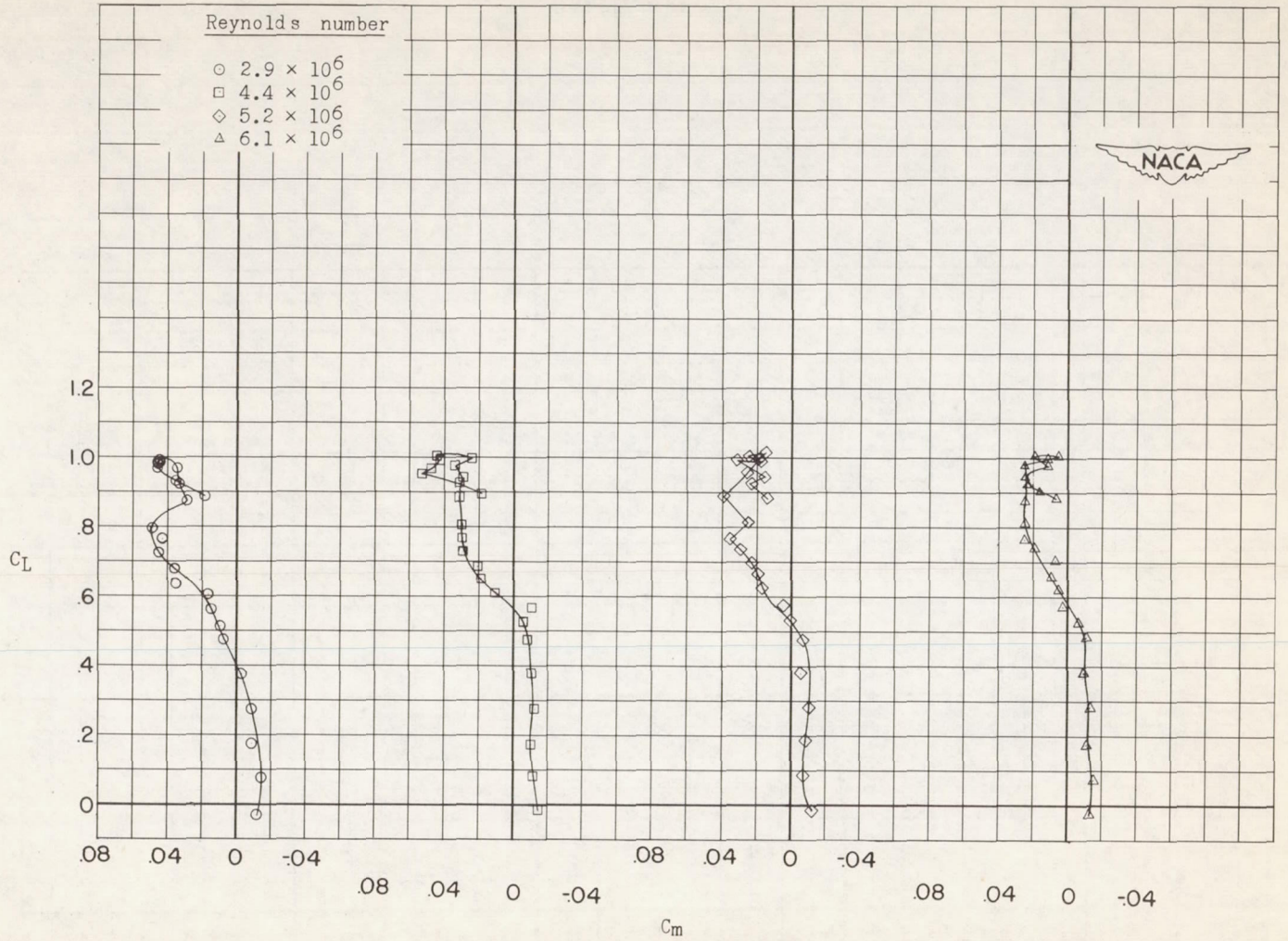
(a) C_L against α.

Figure 8.- Effect of Reynolds number on the aerodynamic characteristics of the semispan 49.1° sweptback wing with 0.50b/2 slat installed. $\delta_s = 45°$.



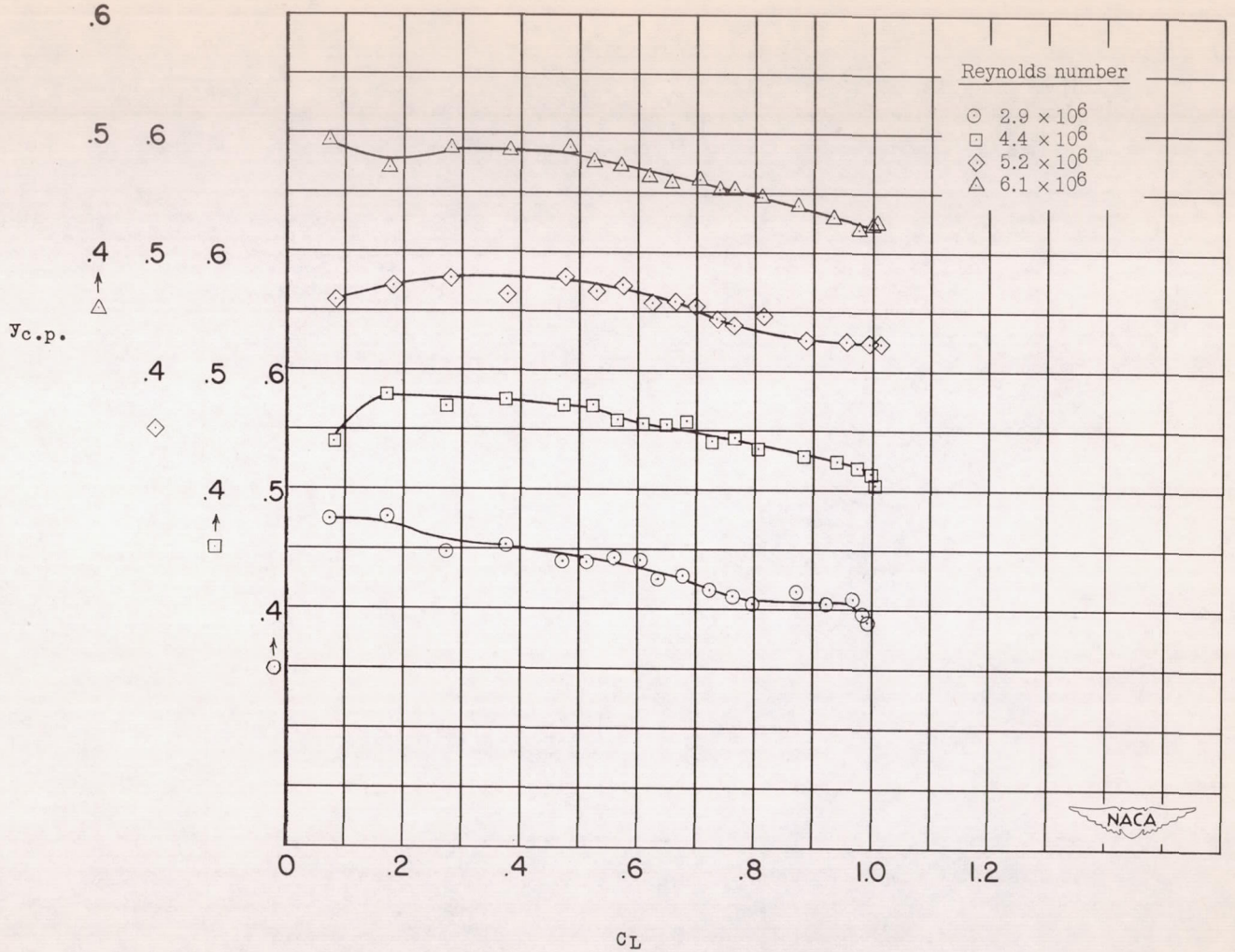
(b) C_D against C_L.

Figure 8.- Continued.



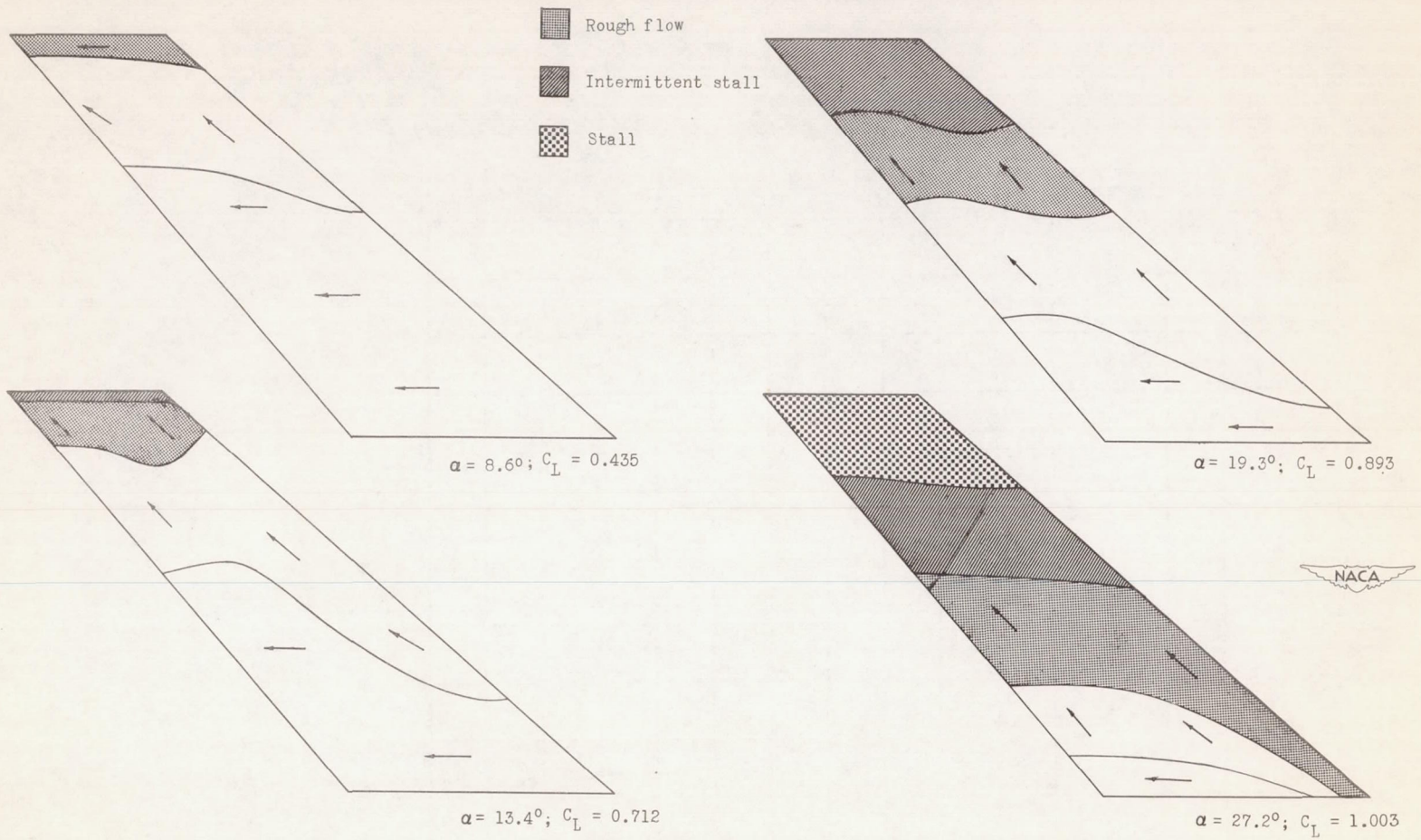
(c) C_m against C_L.

Figure 8.- Continued.



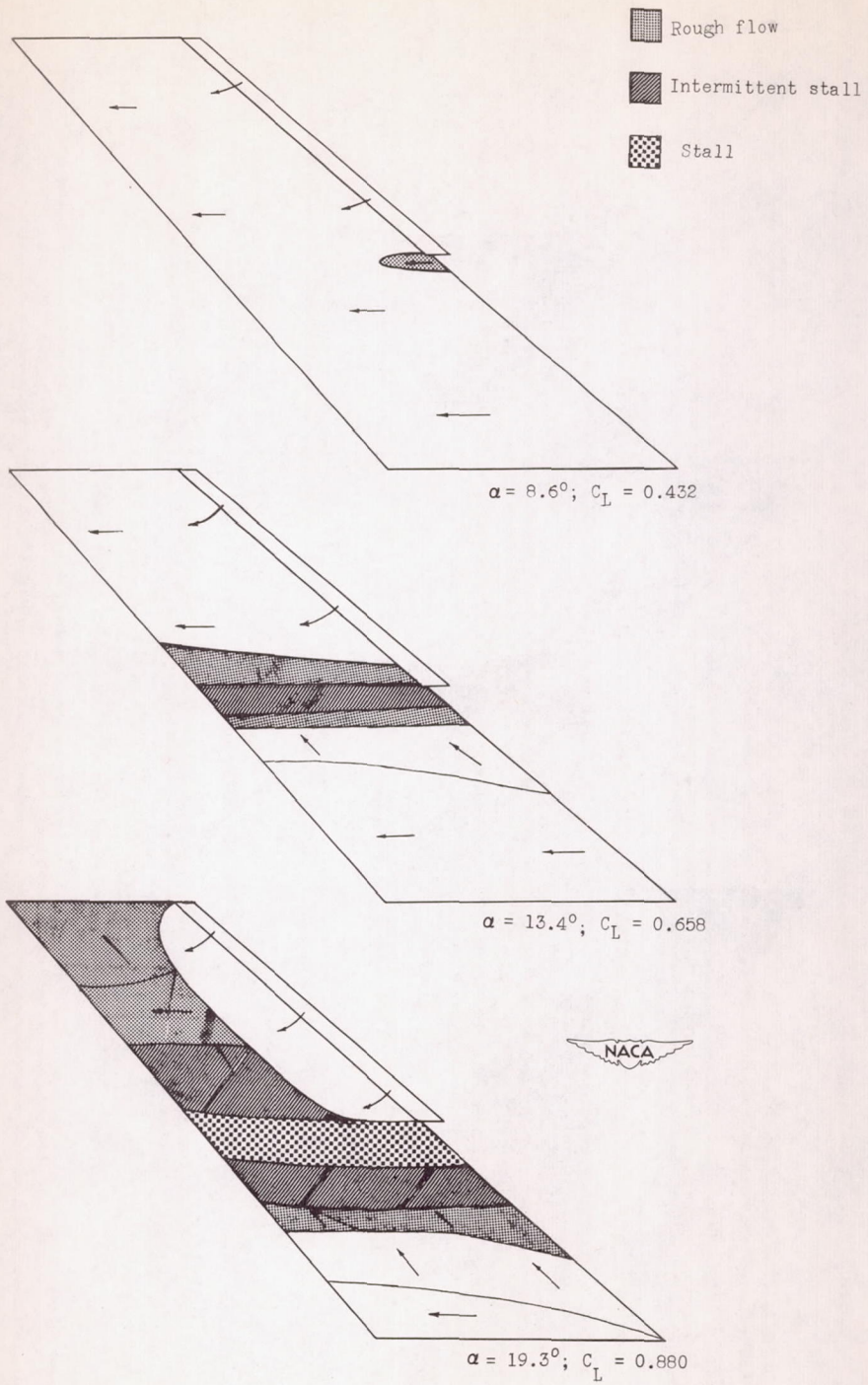
(d) $y_{c.p.}$ against C_L.

Figure 8.- Concluded.



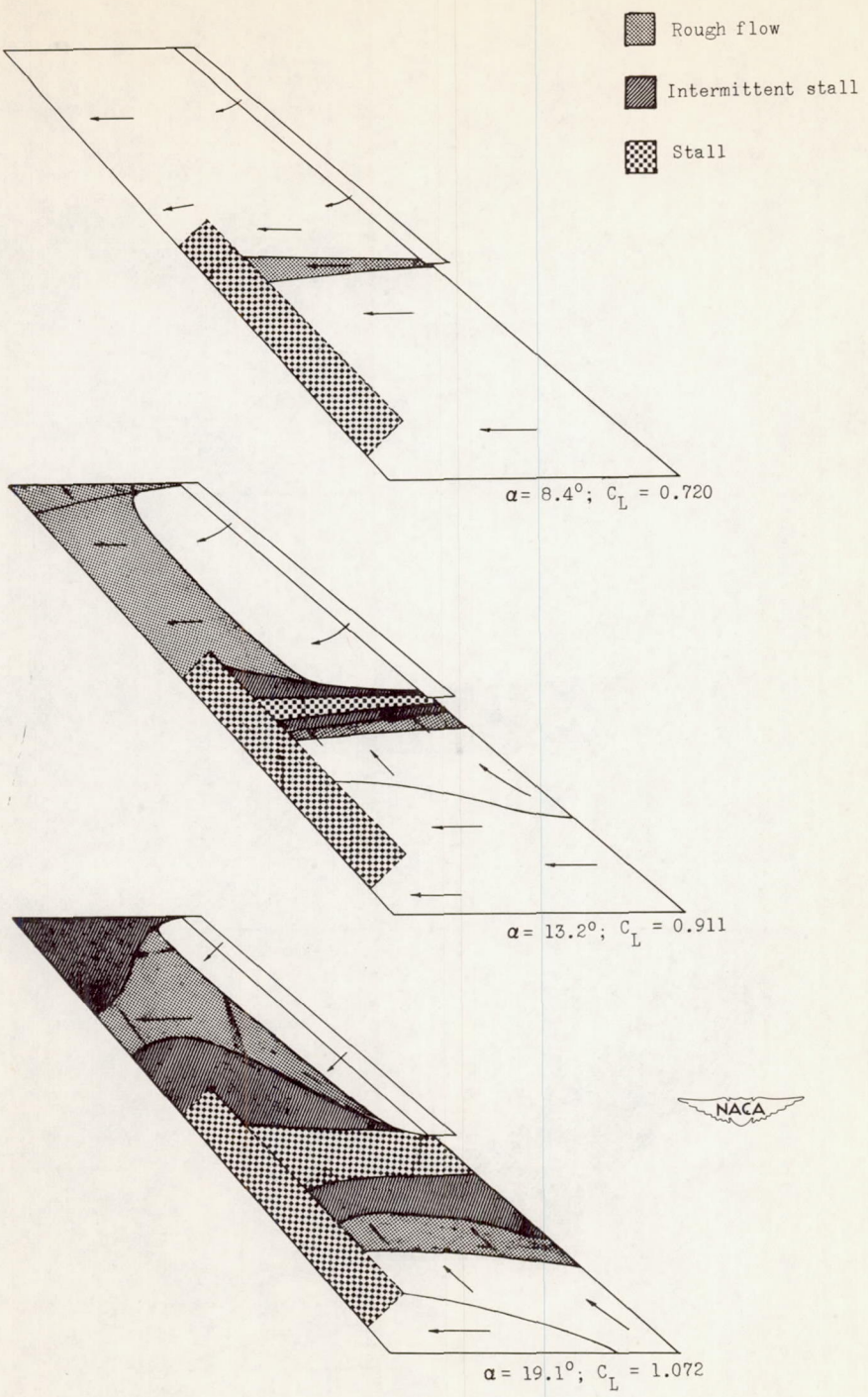
(a) Basic wing.

Figure 9.- Stall characteristics of the semispan 49.1° sweptback wing. $R = 6.1 \times 10^6$.



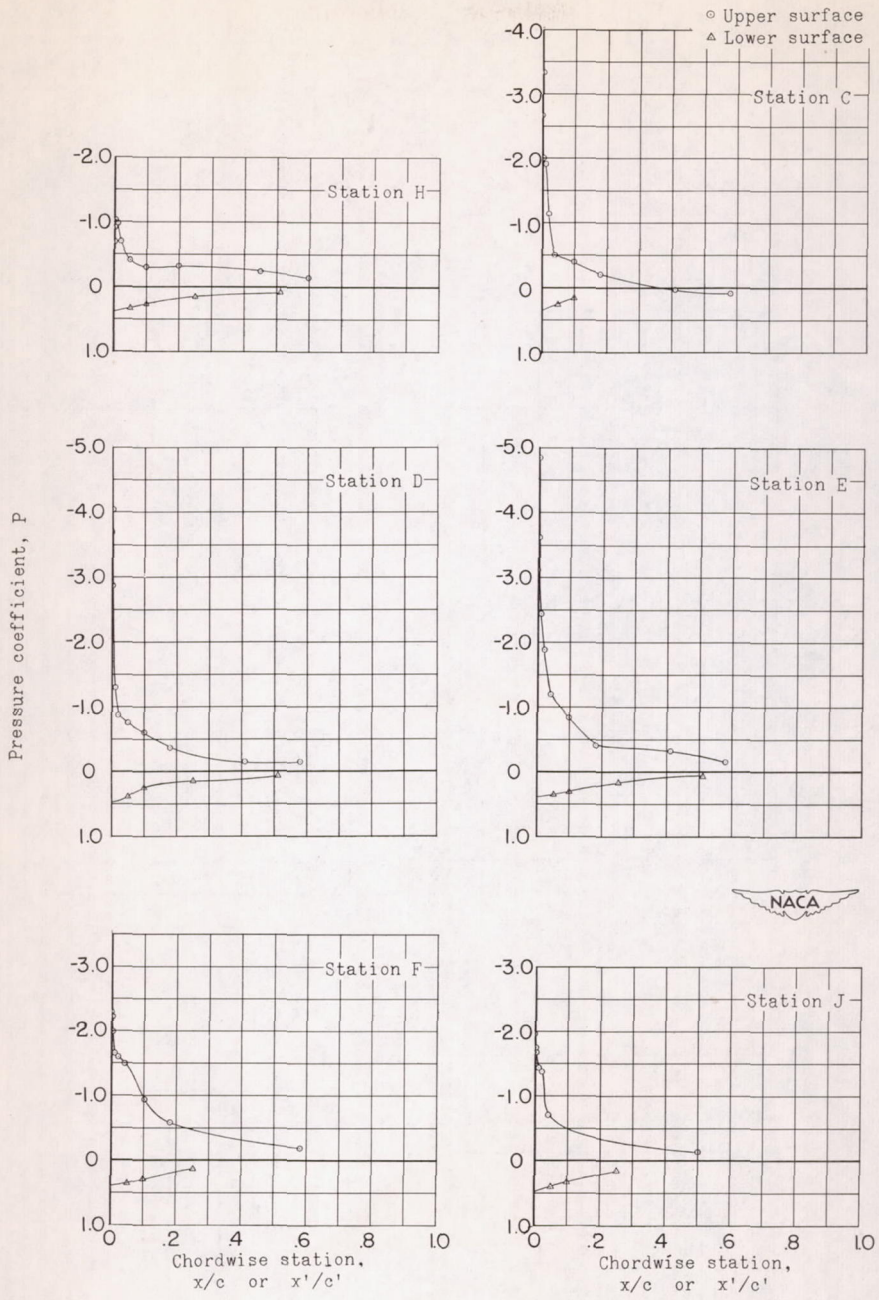
(b) Wing with 0.50b/2 slat installed (δ_s = 45°).

Figure 9.- Continued.



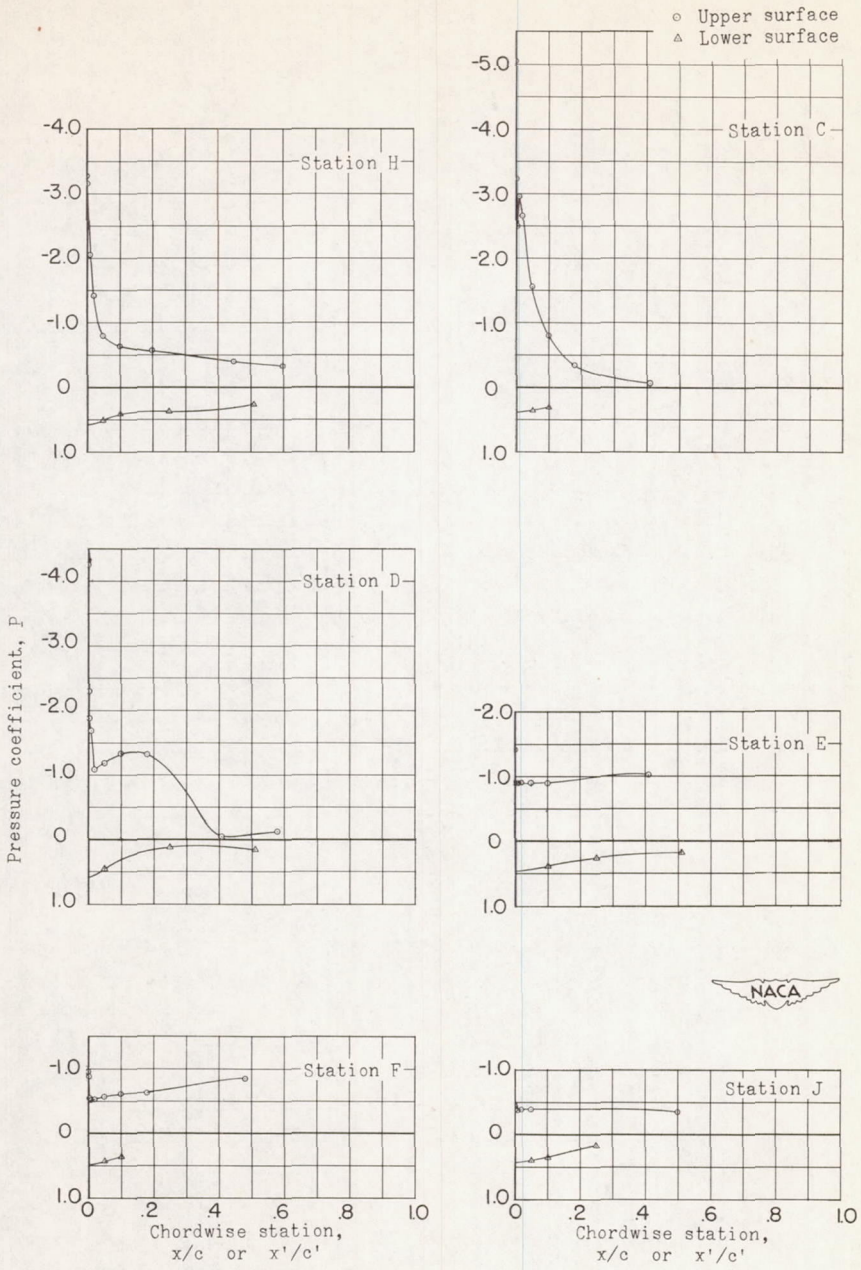
(c) Wing with 0.50b/2 slat installed (δ_s = 45°) and trailing-edge flap deflected.

Figure 9.- Concluded.



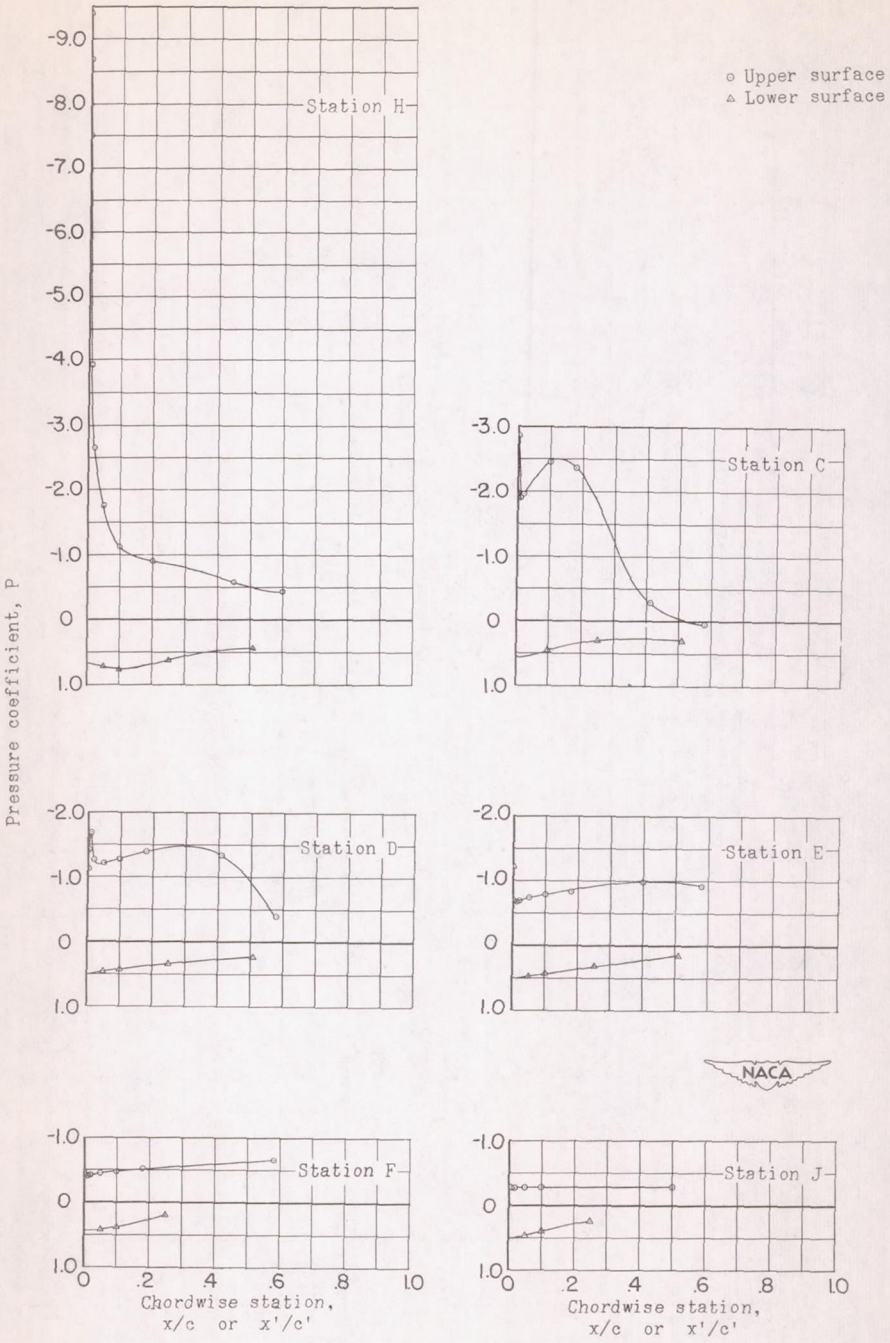
(a) $\alpha = 8.6^{\circ}$; $C_L = 0.435$.

Figure 10.- Wing chordwise pressure distributions for the semispan 49.1° sweptback wing; basic wing. $R = 6.1 \times 10^6$.



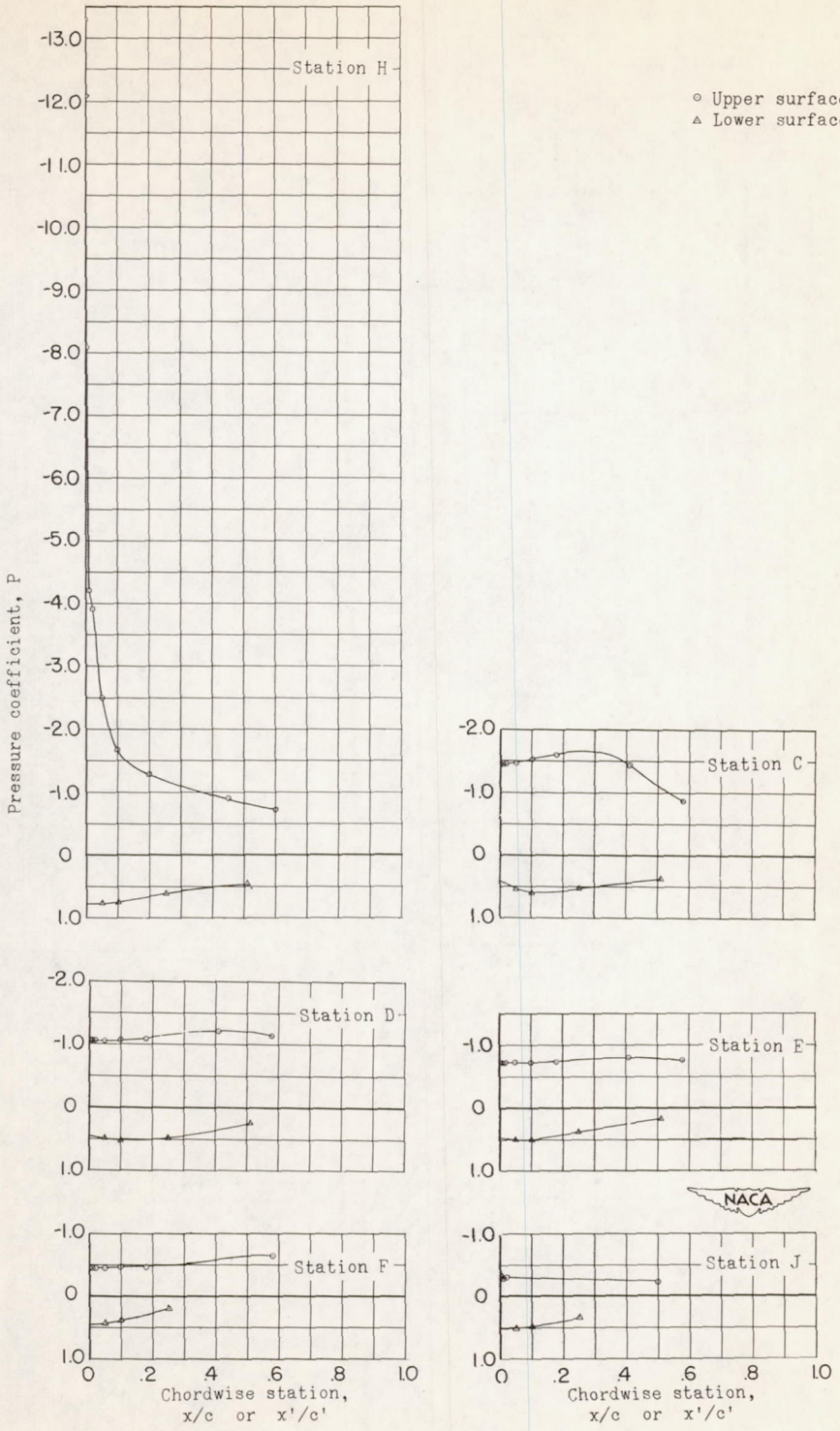
(b) $\alpha = 13.4^{\circ}$; $C_L = 0.712$.

Figure 10.- Continued.



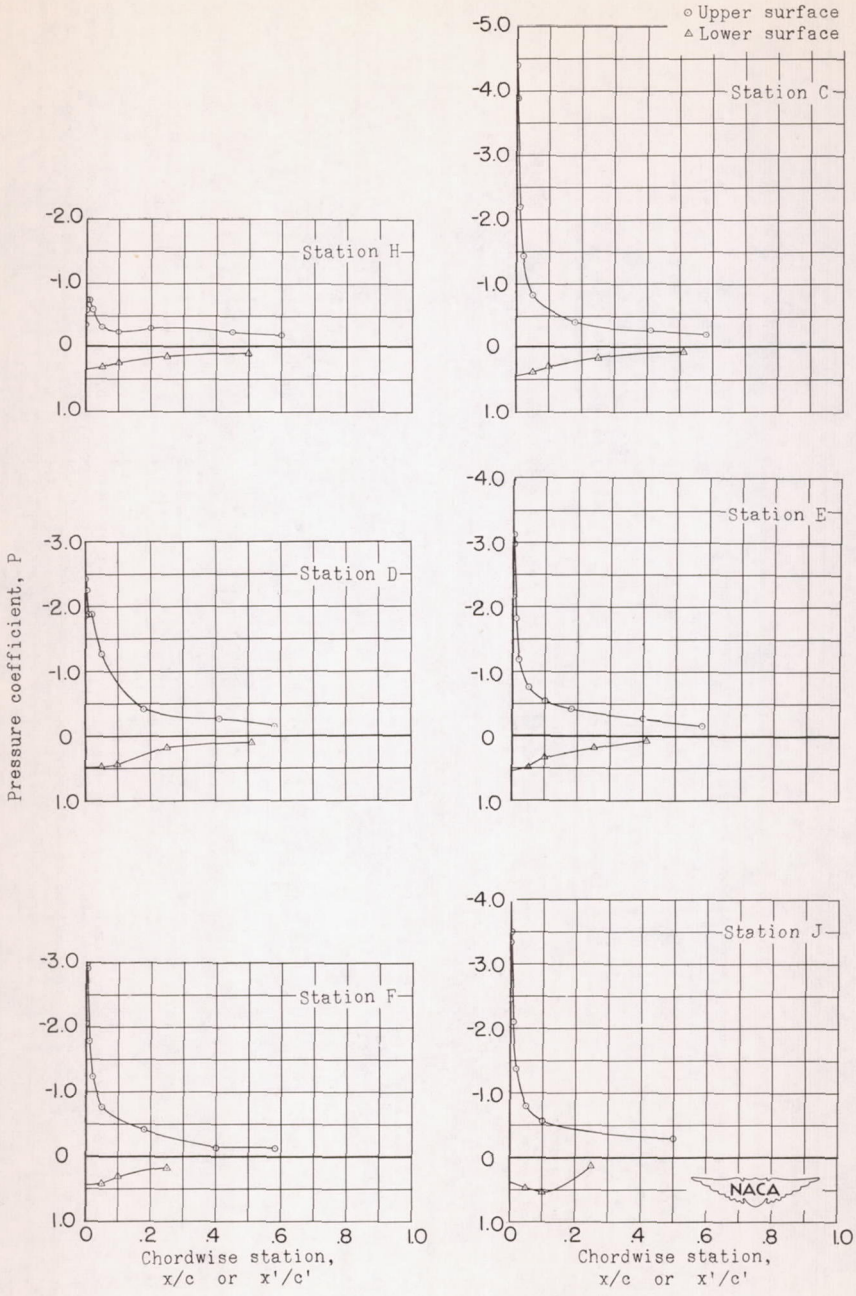
(c) $\alpha = 19.3^{\circ}$; $C_L = 0.893$.

Figure 10.- Continued.



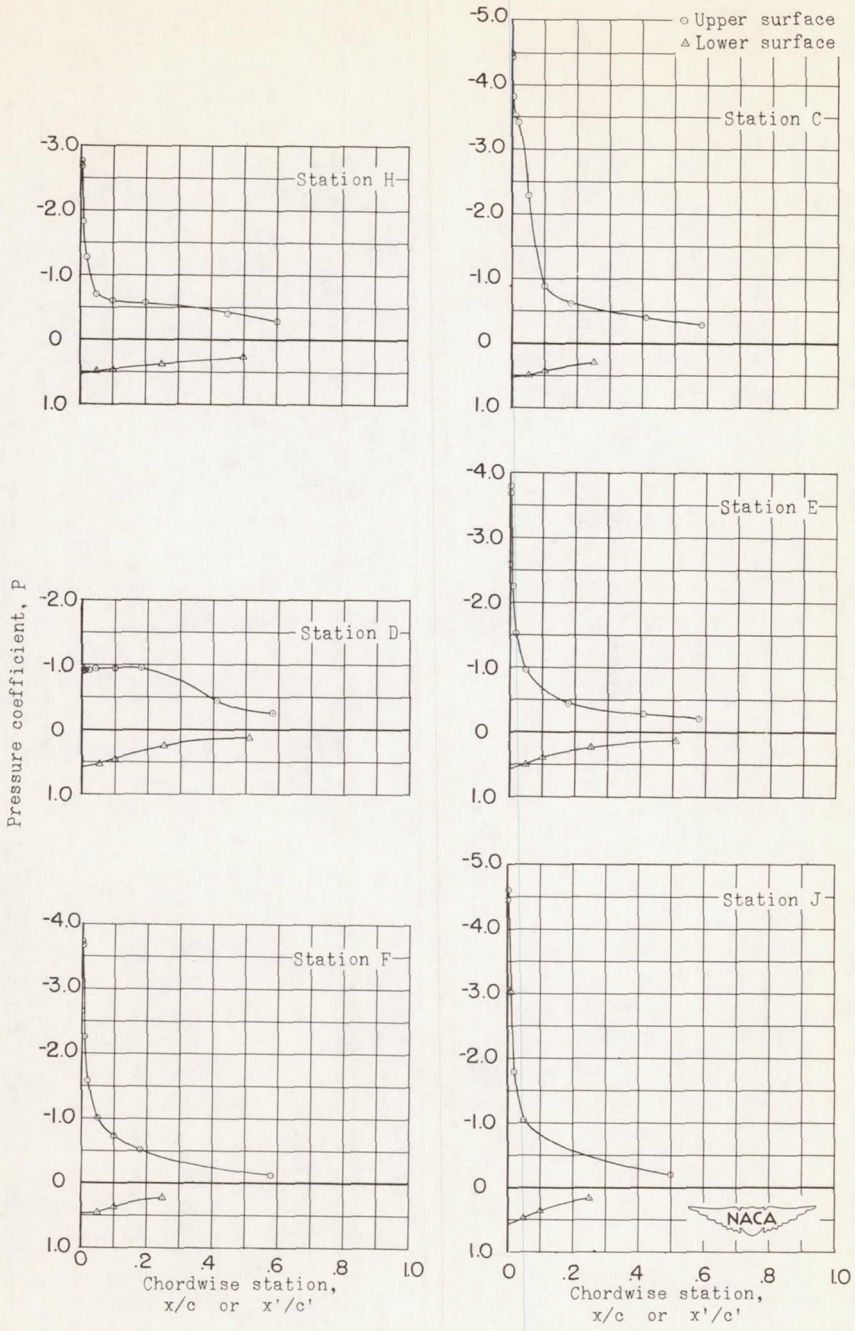
(d) $\alpha = 27.2^{\circ}$; $C_L = 1.003$.

Figure 10.- Concluded.



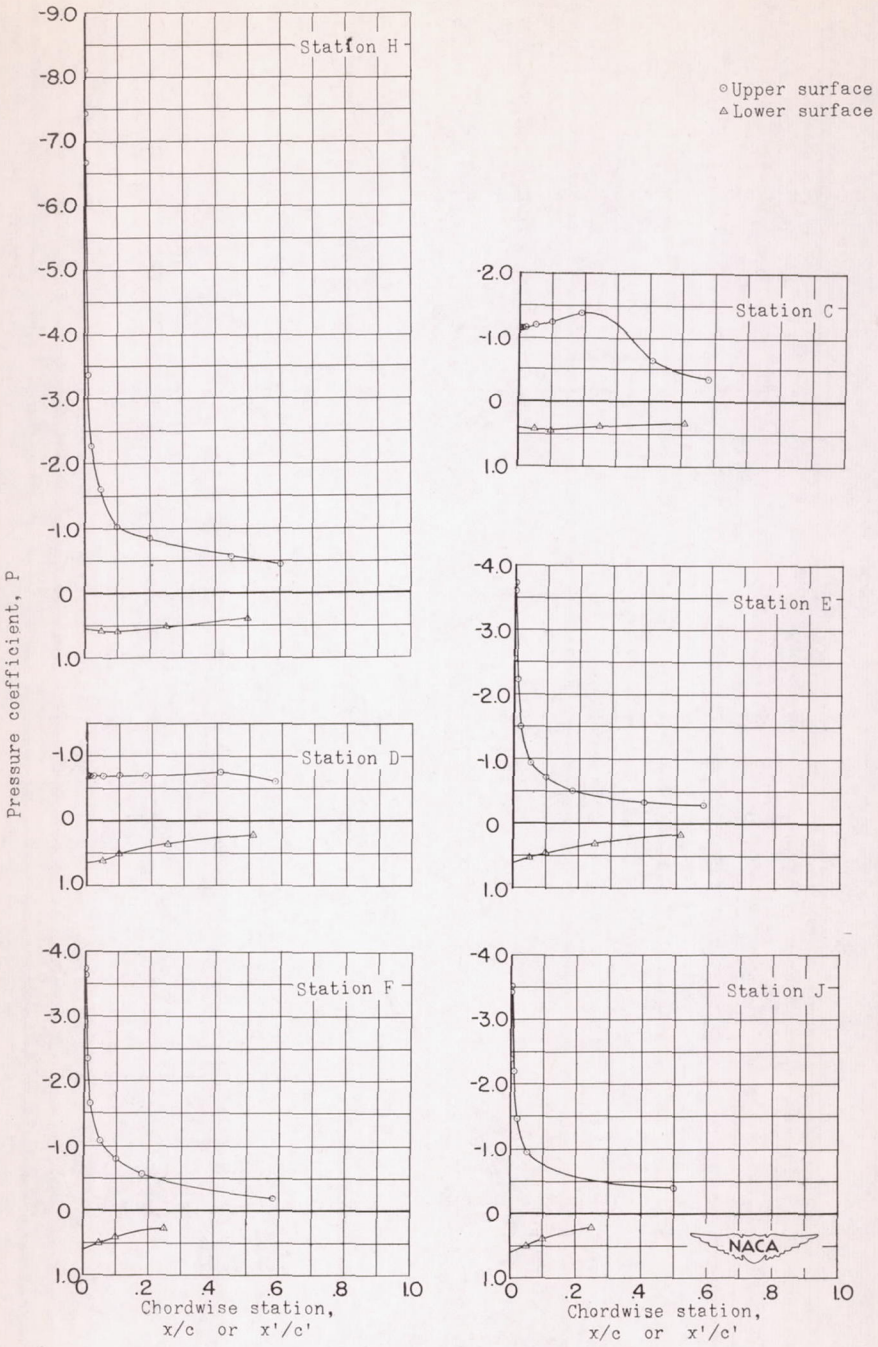
(a) $\alpha = 8.6^{\circ}$; $C_L = 0.432$.

Figure 11.- Wing chordwise pressure distributions for the semispan 49.1° sweptback wing with 0.50b/2 slat installed. $\delta_s = 45^{\circ}$; $R = 6.1 \times 10^6$.



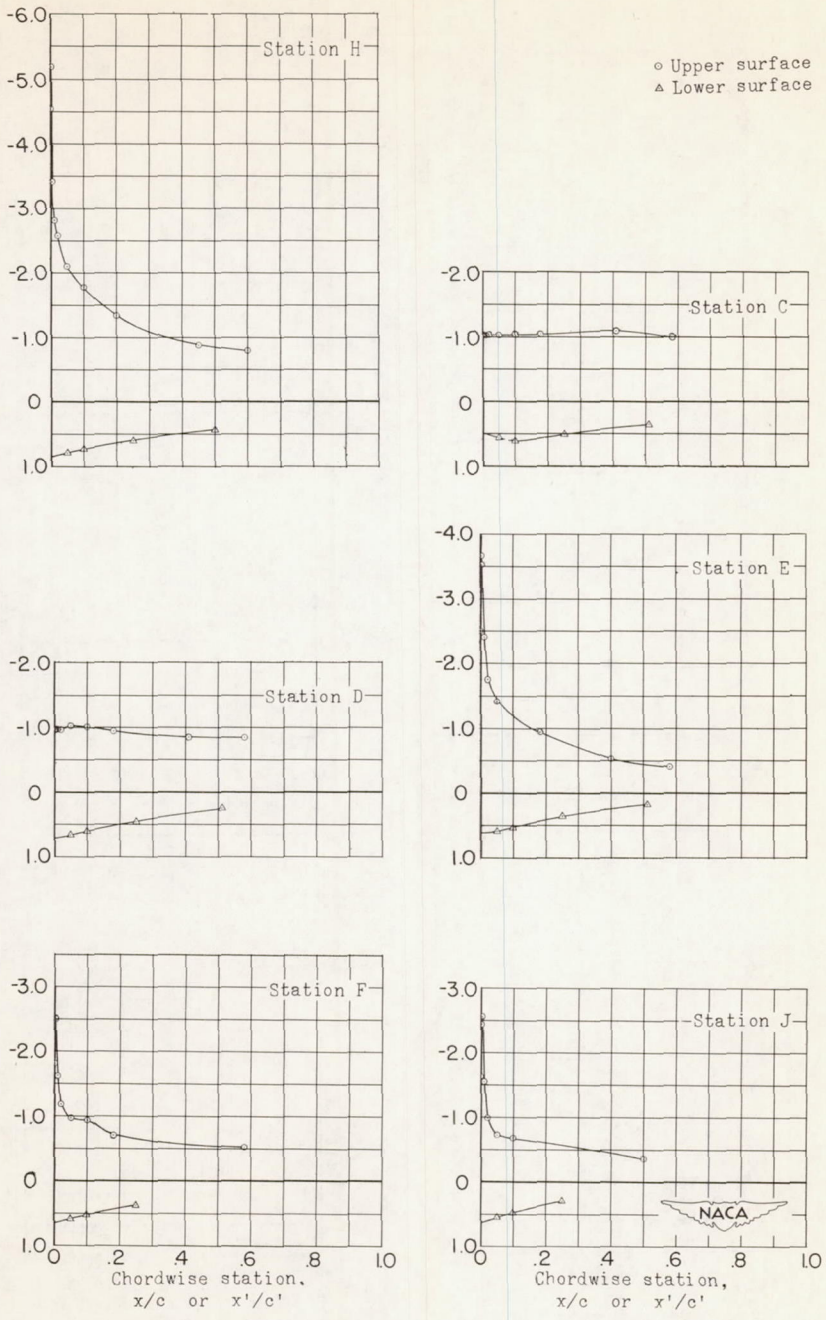
(b) $\alpha = 13.4^{\circ}$; $C_L = 0.658$.

Figure 11.- Continued.



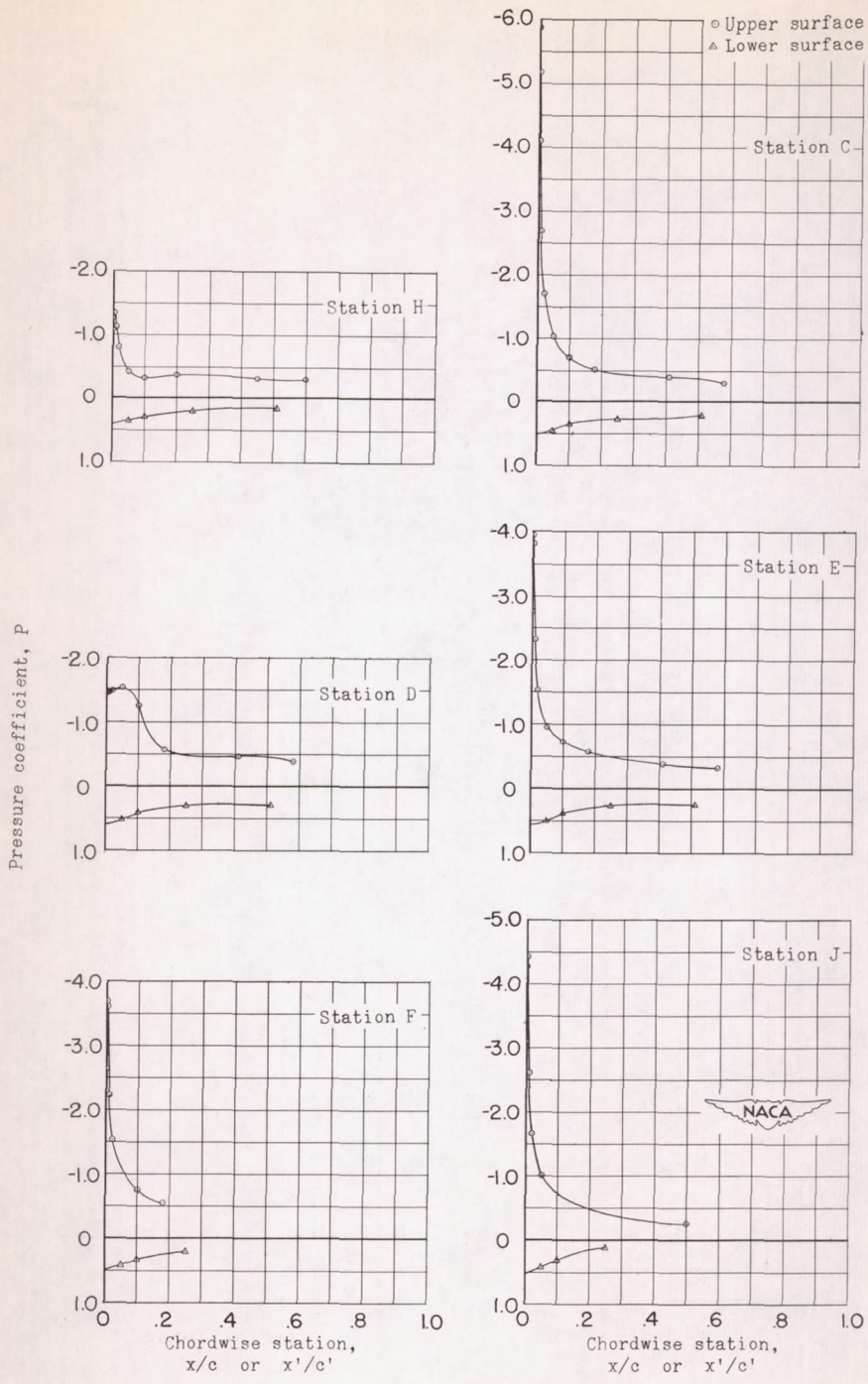
(c) $\alpha = 19.3^{\circ}$; $C_L = 0.880$.

Figure 11.- Continued.



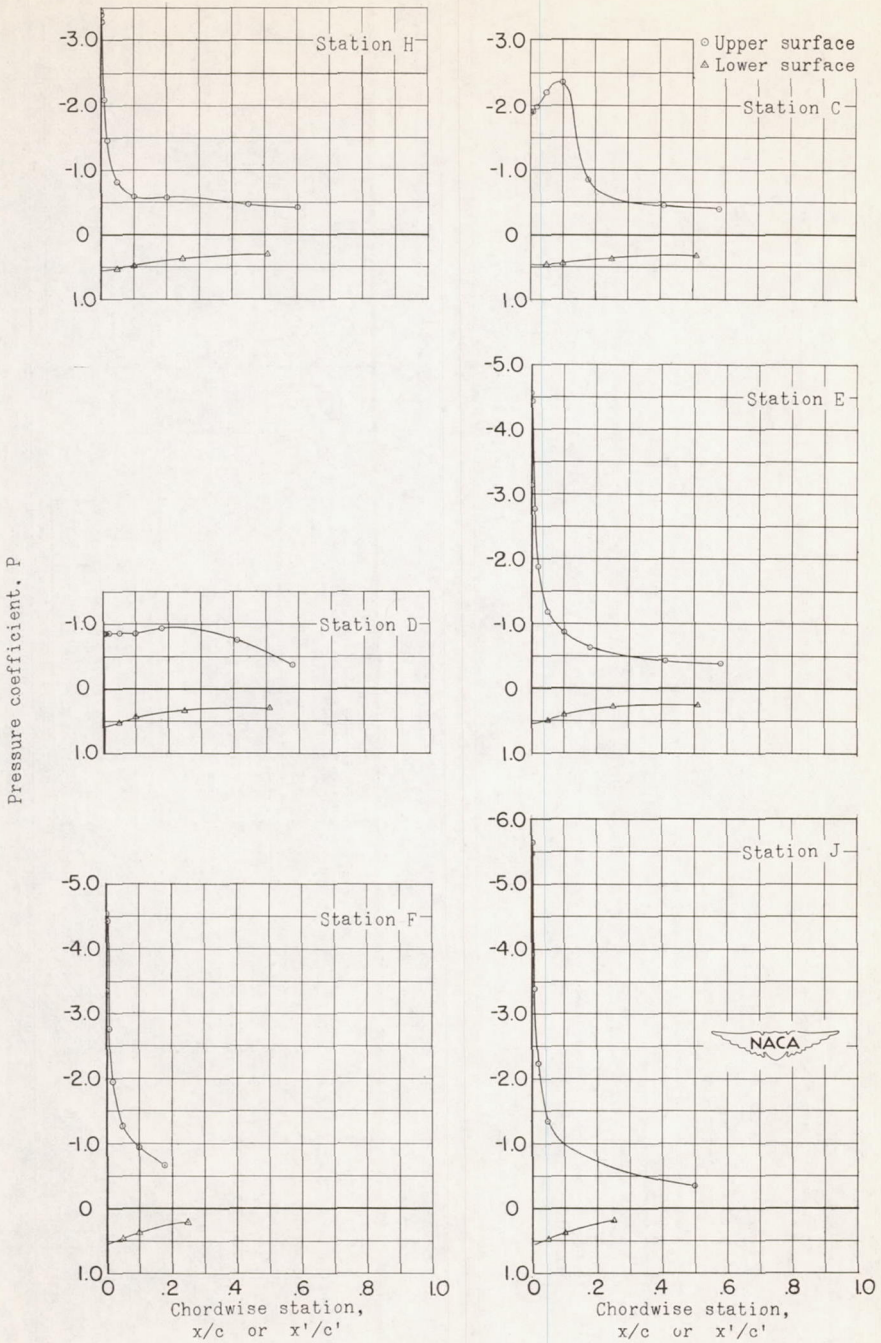
(d) $\alpha = 27.2^{\circ}$; $C_L = 1.002$.

Figure 11.- Concluded.



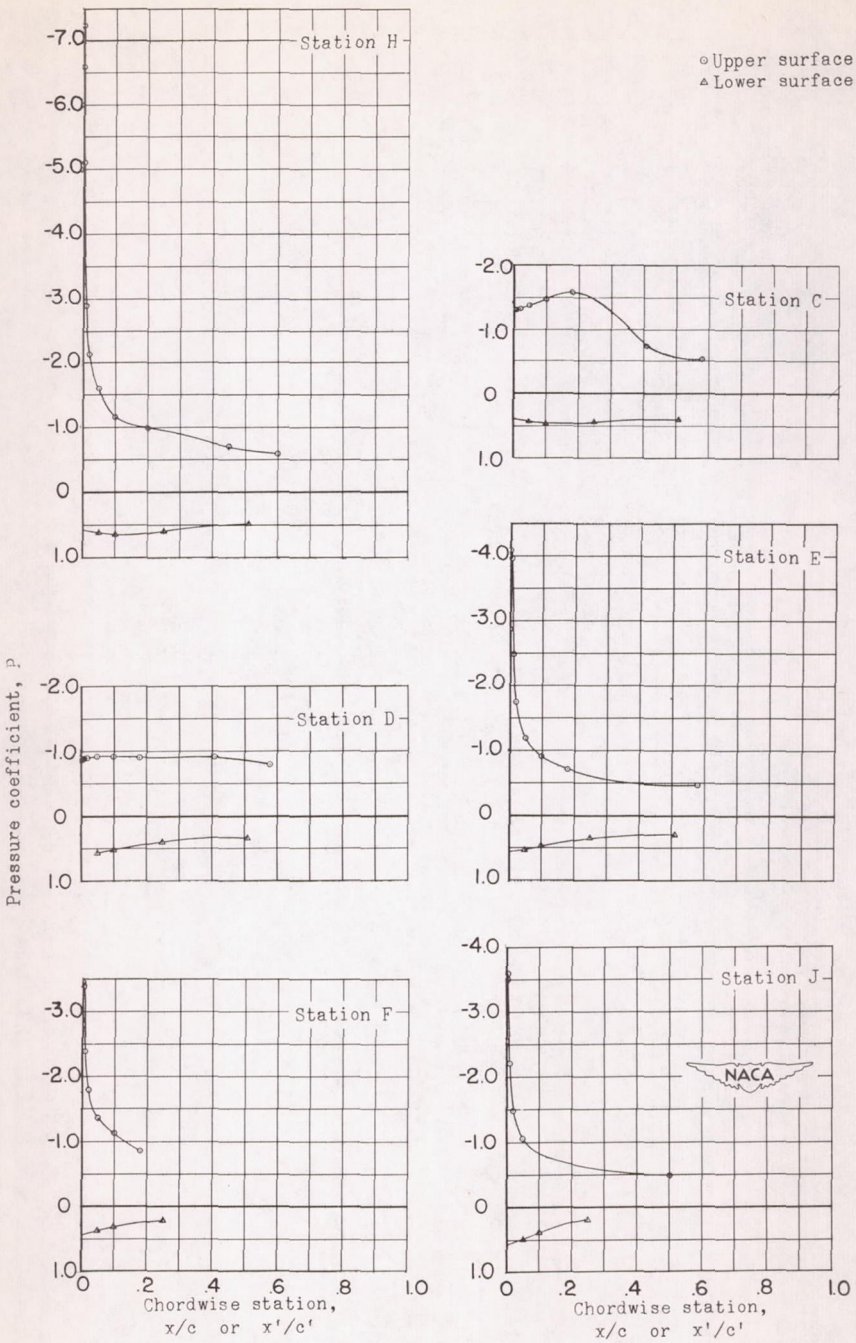
(a) $\alpha = 8.4^{\circ}$; $C_L = 0.720$.

Figure 12.- Wing chordwise pressure distributions for the semispan 49.1° sweptback wing with 0.50b/2 slat installed and trailing-edge flap deflected. $\delta_s = 45^{\circ}$; $R = 6.1 \times 10^6$.



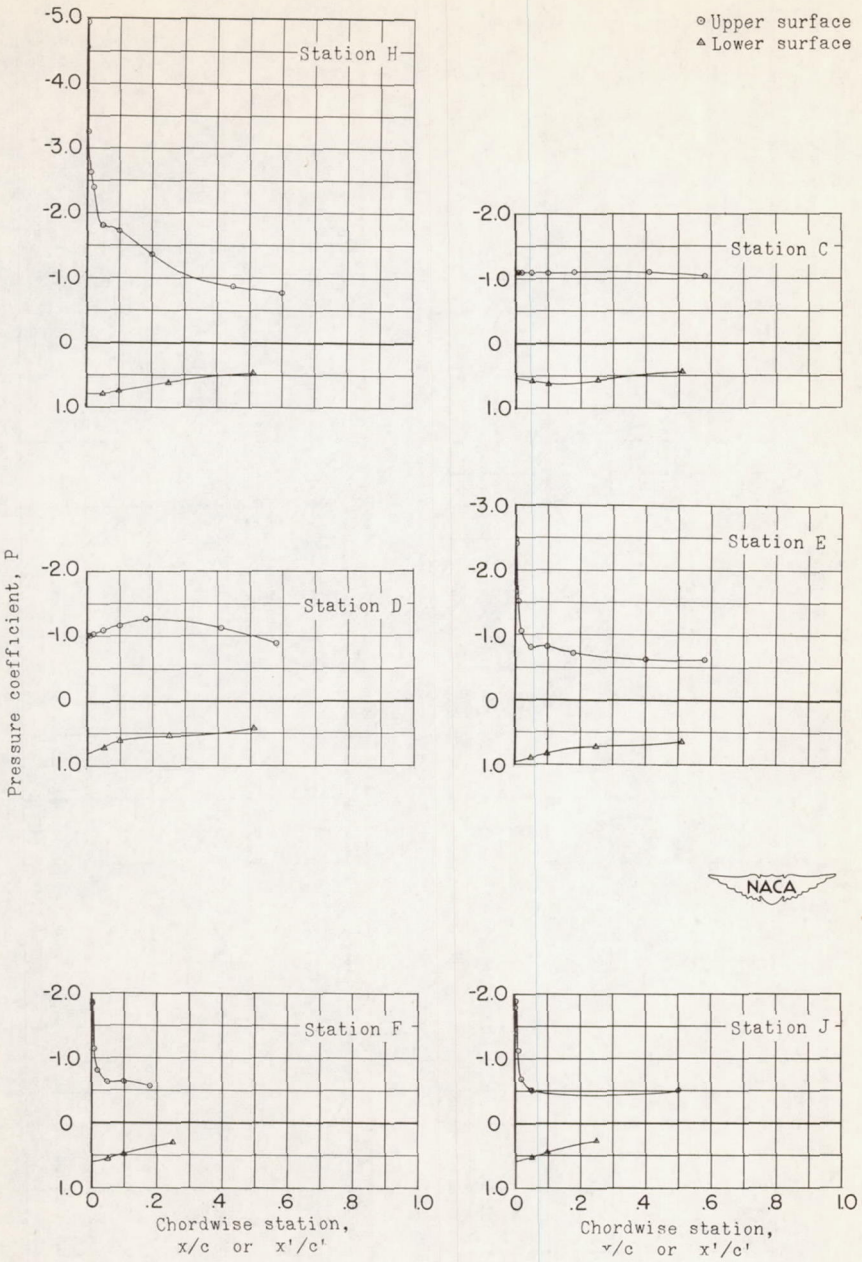
(b) $\alpha = 13.2^{\circ}$; $C_L = 0.911$.

Figure 12.- Continued.



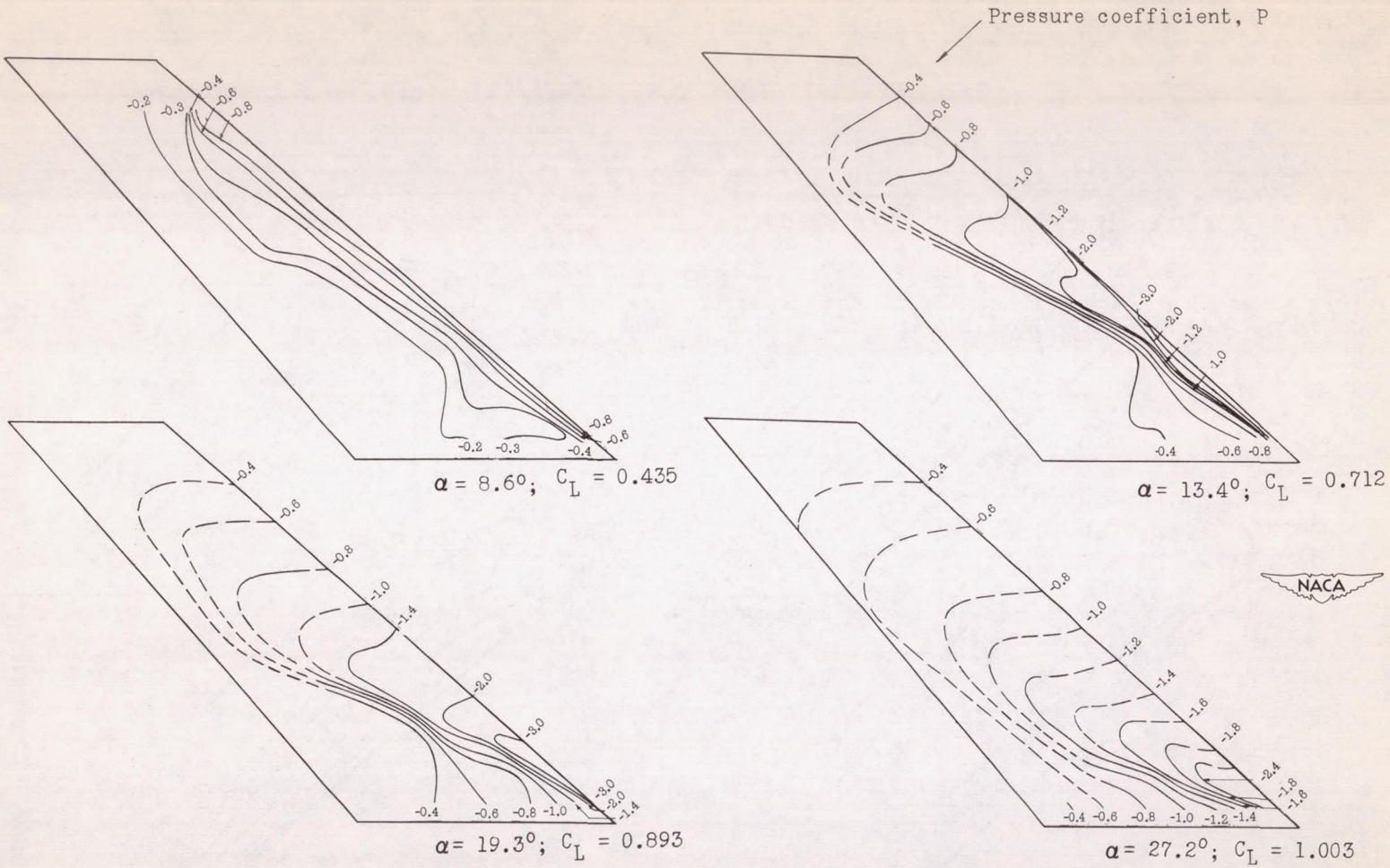
(c) $\alpha = 19.1^{\circ}$; $C_L = 1.072$.

Figure 12.- Continued.



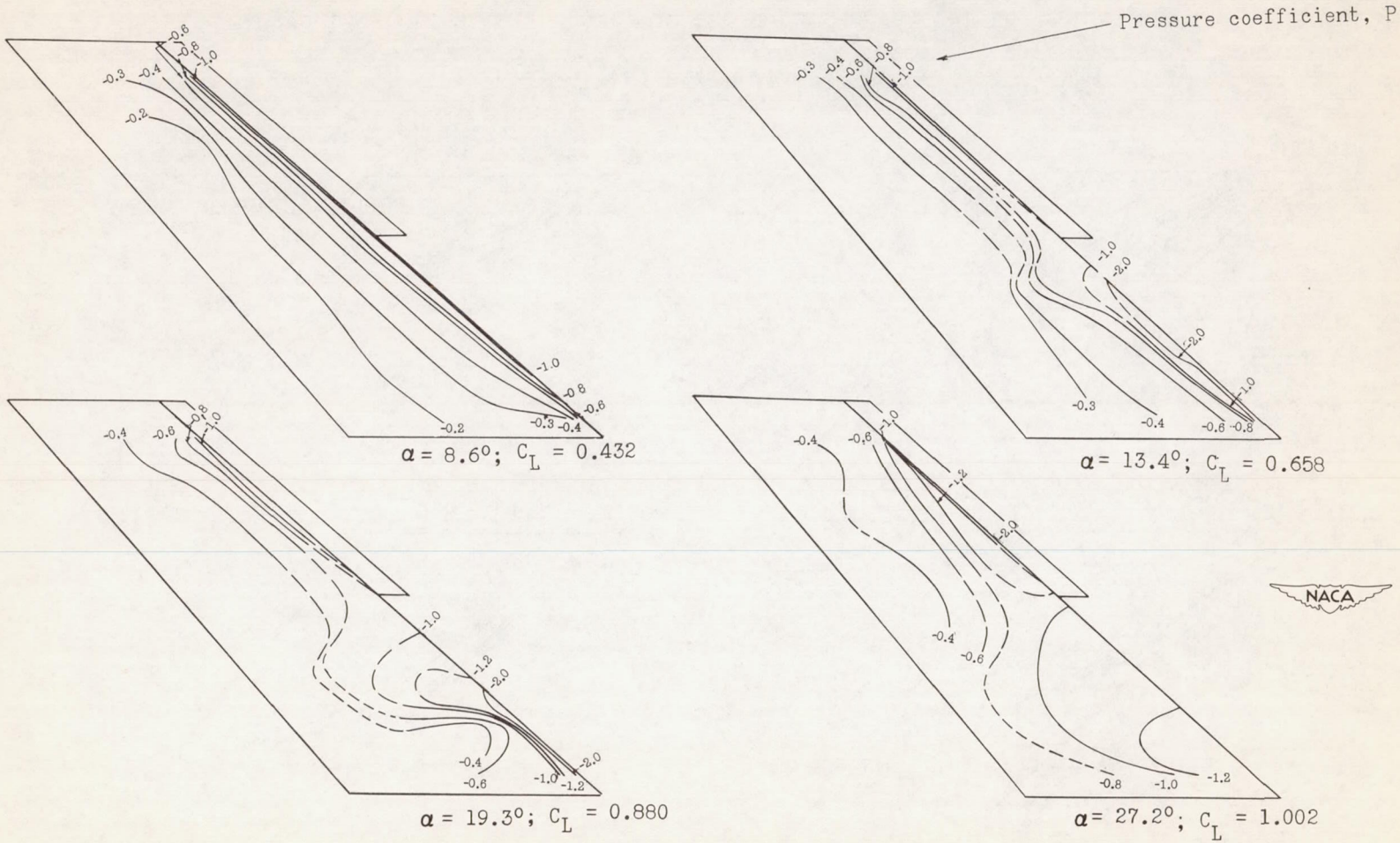
(d) $\alpha = 27.1^{\circ}$; $C_L = 1.020$.

Figure 12.- Concluded.



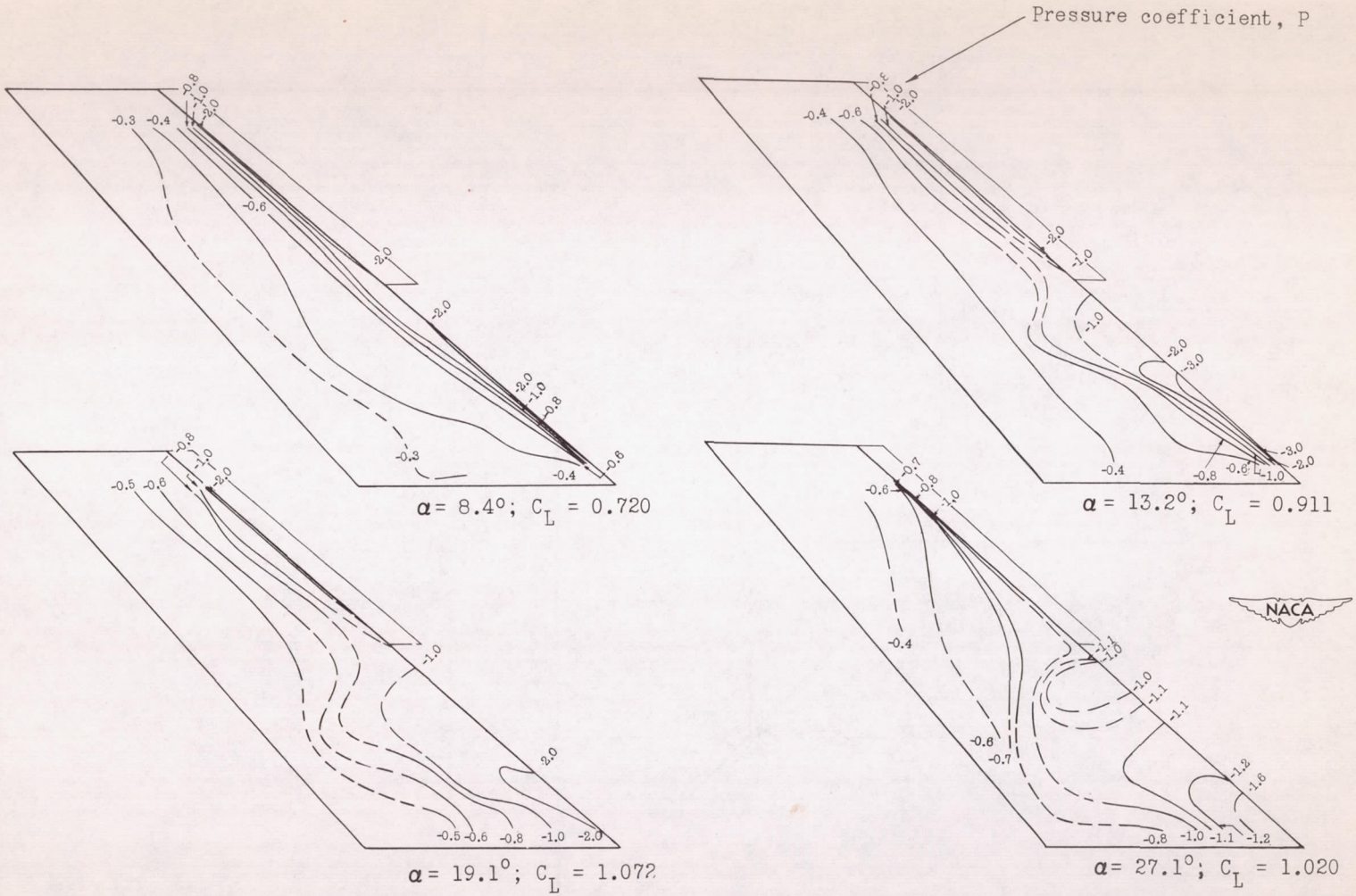
(a) Basic wing.

Figure 13.- Pressure isobars for the upper surface of the semispan 49.1° sweptback wing. $R = 6.1 \times 10^6$.



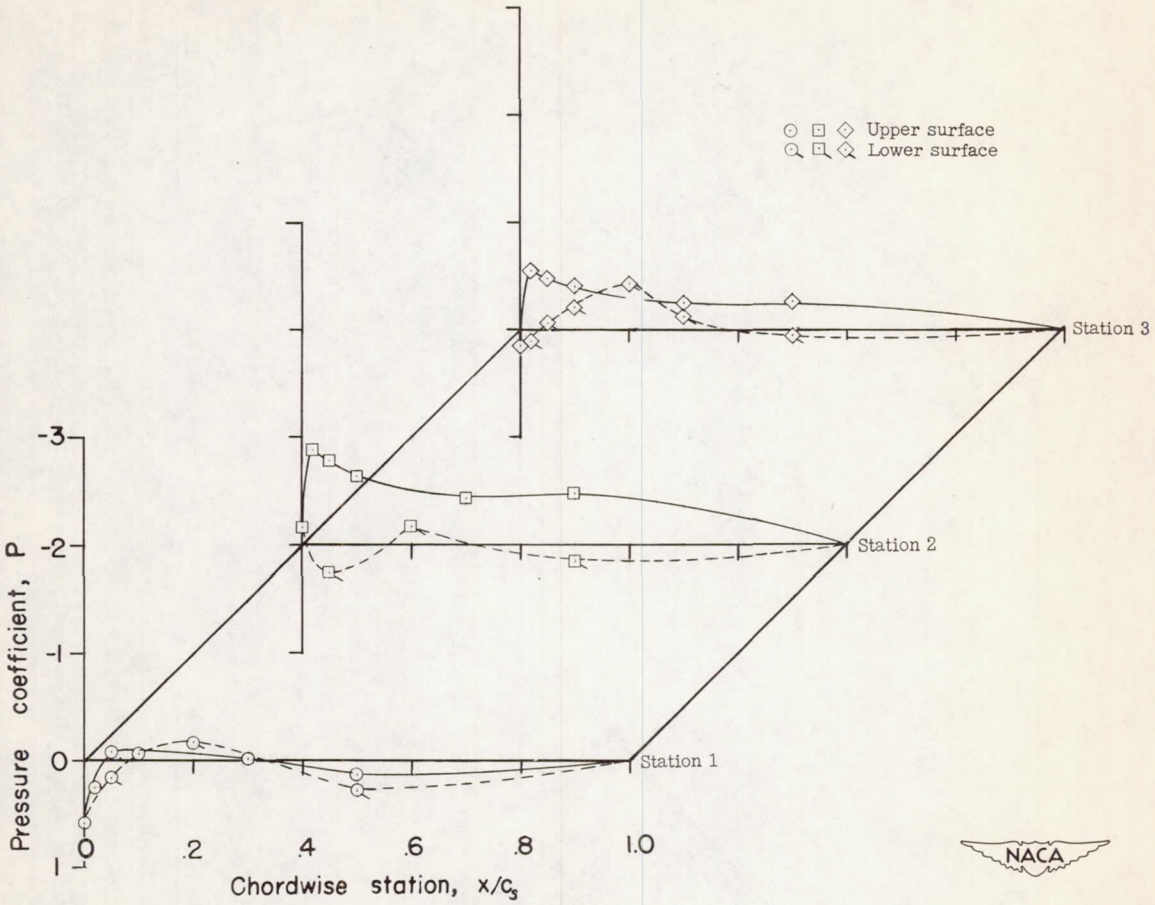
(b) Wing with 0.50b/2 slat installed.

Figure 13.- Continued.



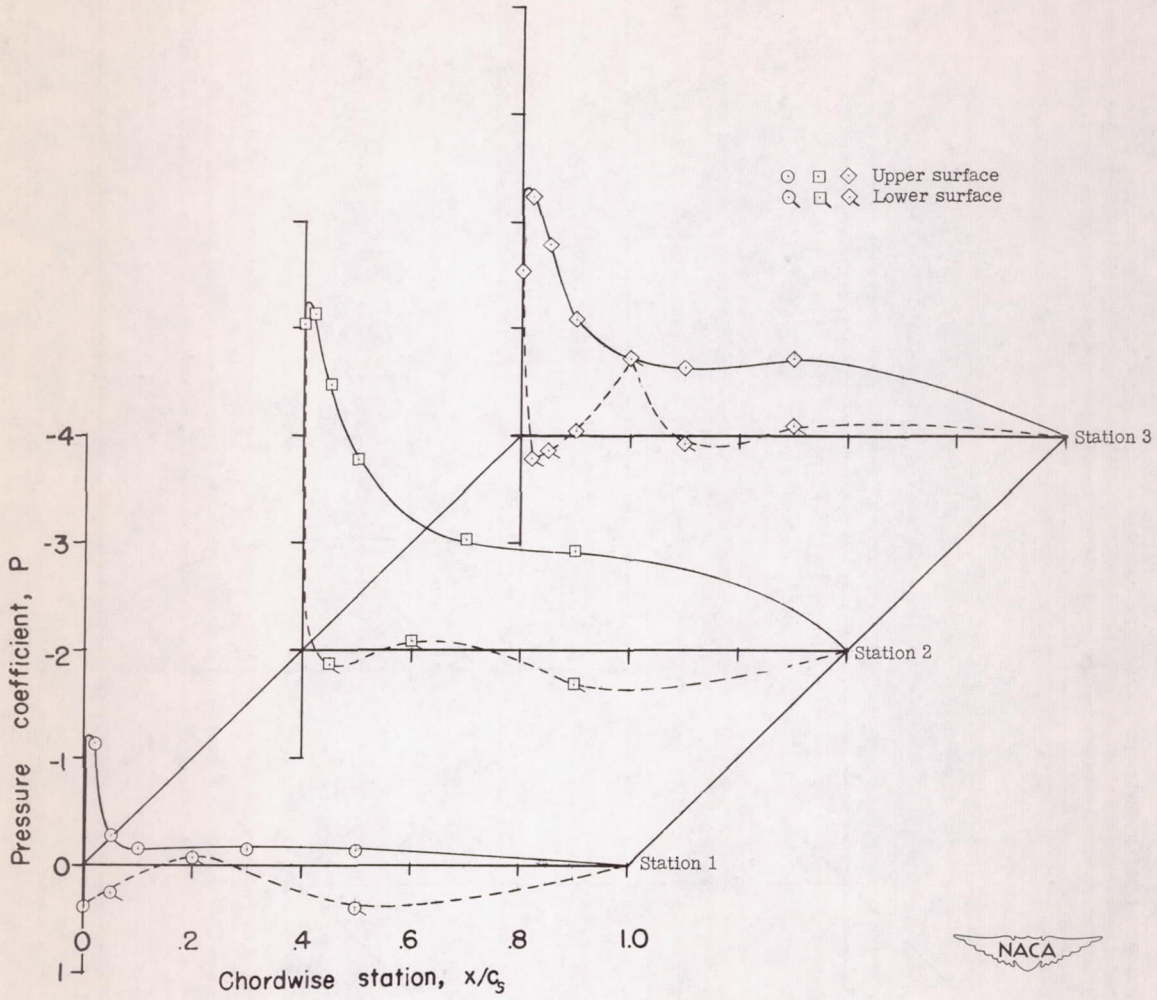
(c) Wing with 0.50b/2 slat installed and trailing-edge flap deflected.

Figure 13.- Concluded.



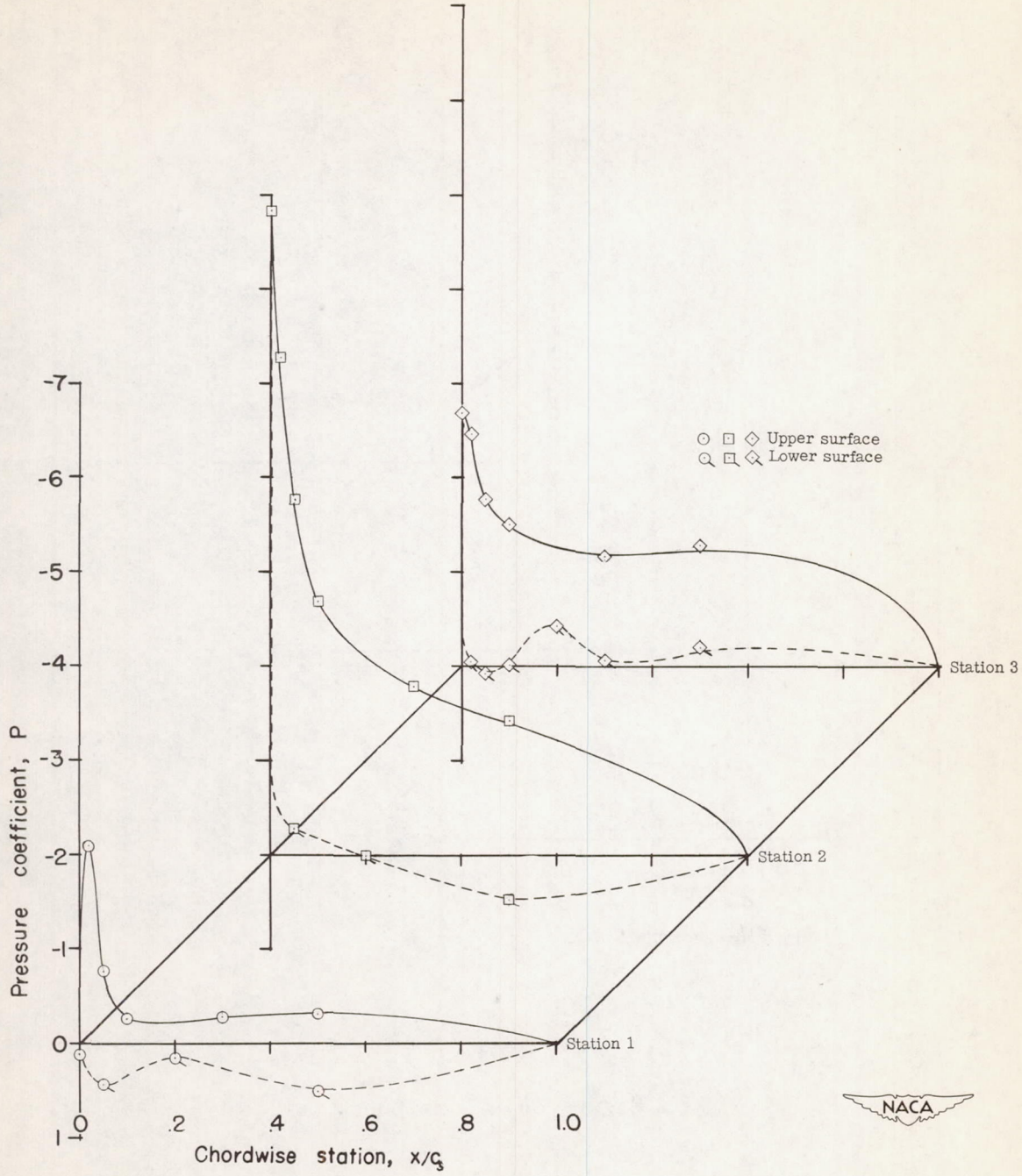
(a) $\alpha = 8.6^{\circ}$; $C_L = 0.432$.

Figure 14.- Slat chordwise pressure distributions for the 0.50b/2 slat installed on the semispan 49.1° sweptback wing. $\delta_s = 45^{\circ}$; $R = 6.1 \times 10^6$.



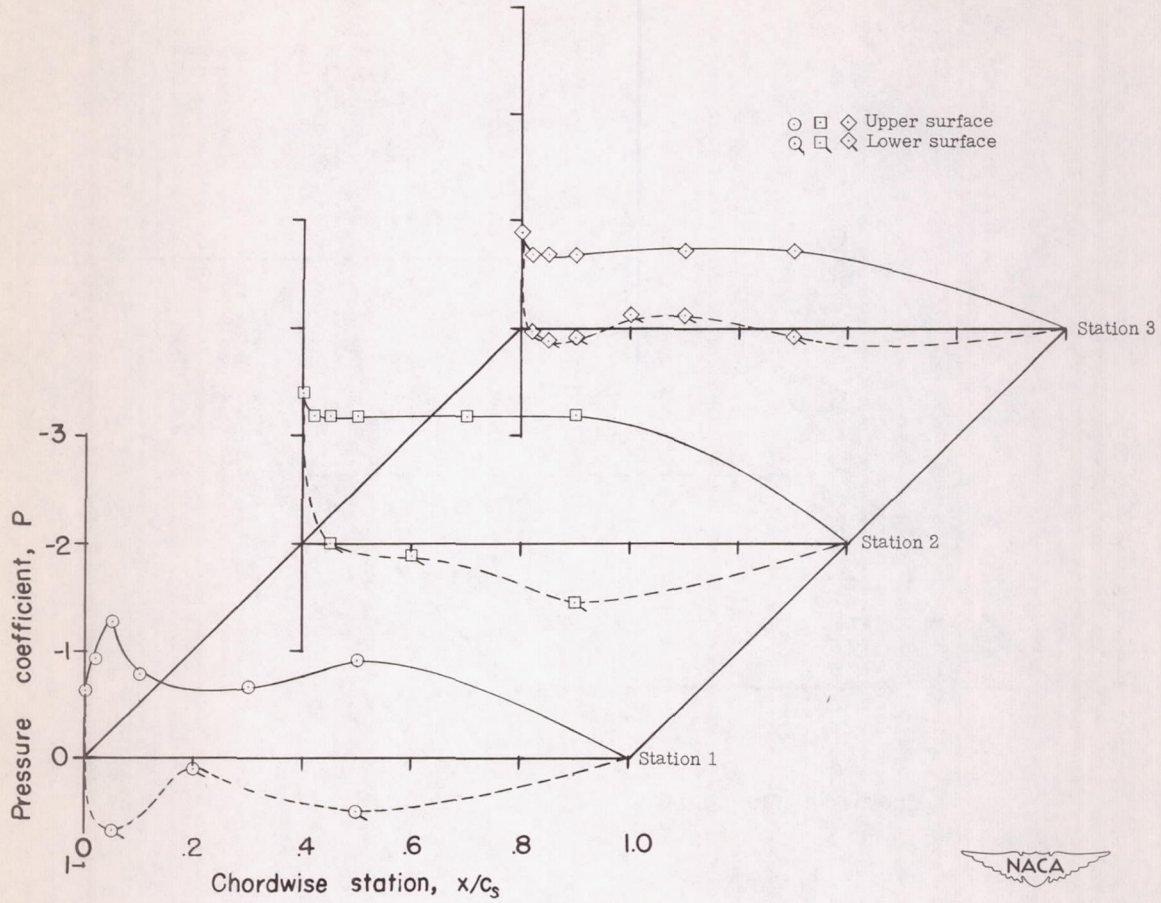
(b) $\alpha = 13.4^{\circ}$; $C_L = 0.658$.

Figure 14.- Continued.



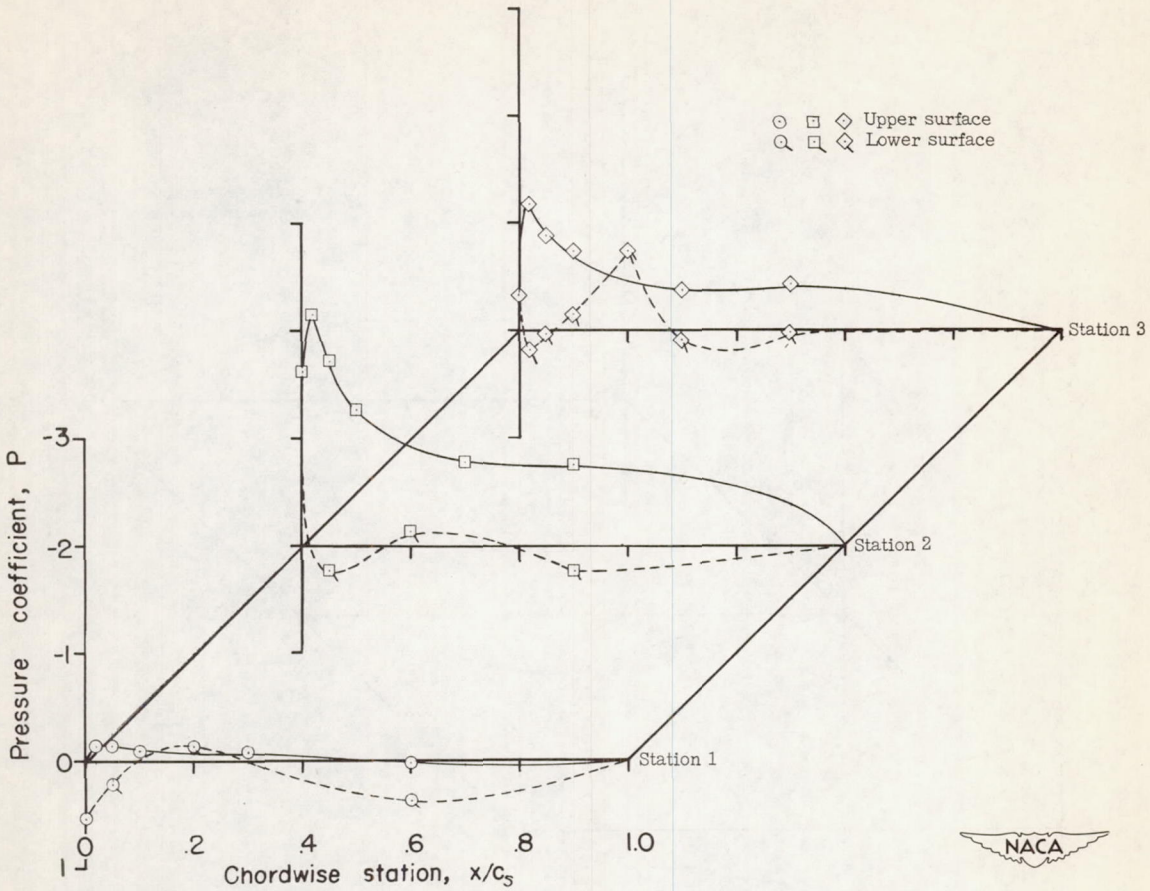
(c) $\alpha = 19.3^{\circ}$; $C_L = 0.880$.

Figure 14.- Continued.



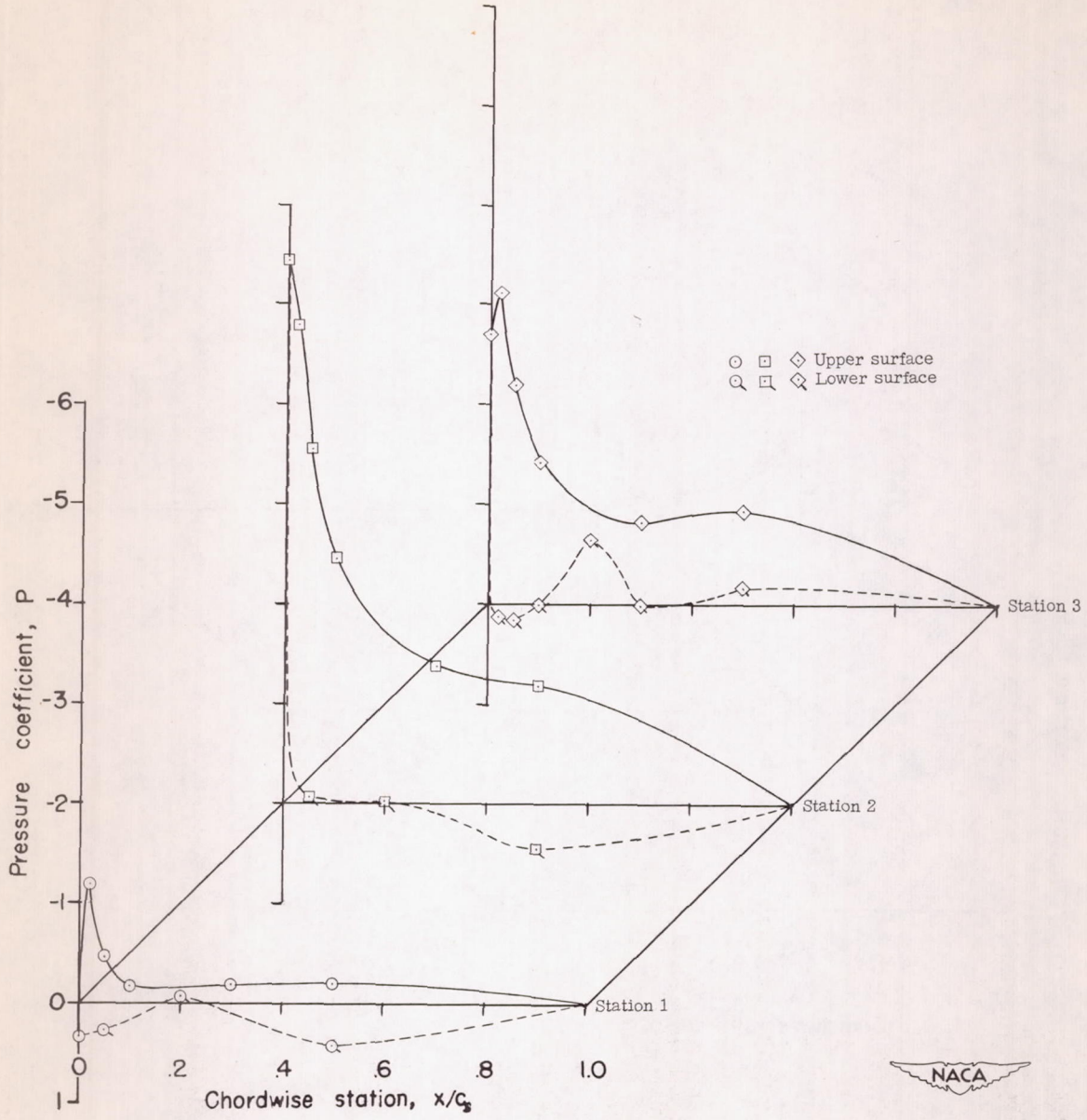
(d) $\alpha = 27.2^{\circ}$; $C_L = 1.002$.

Figure 14.- Concluded.



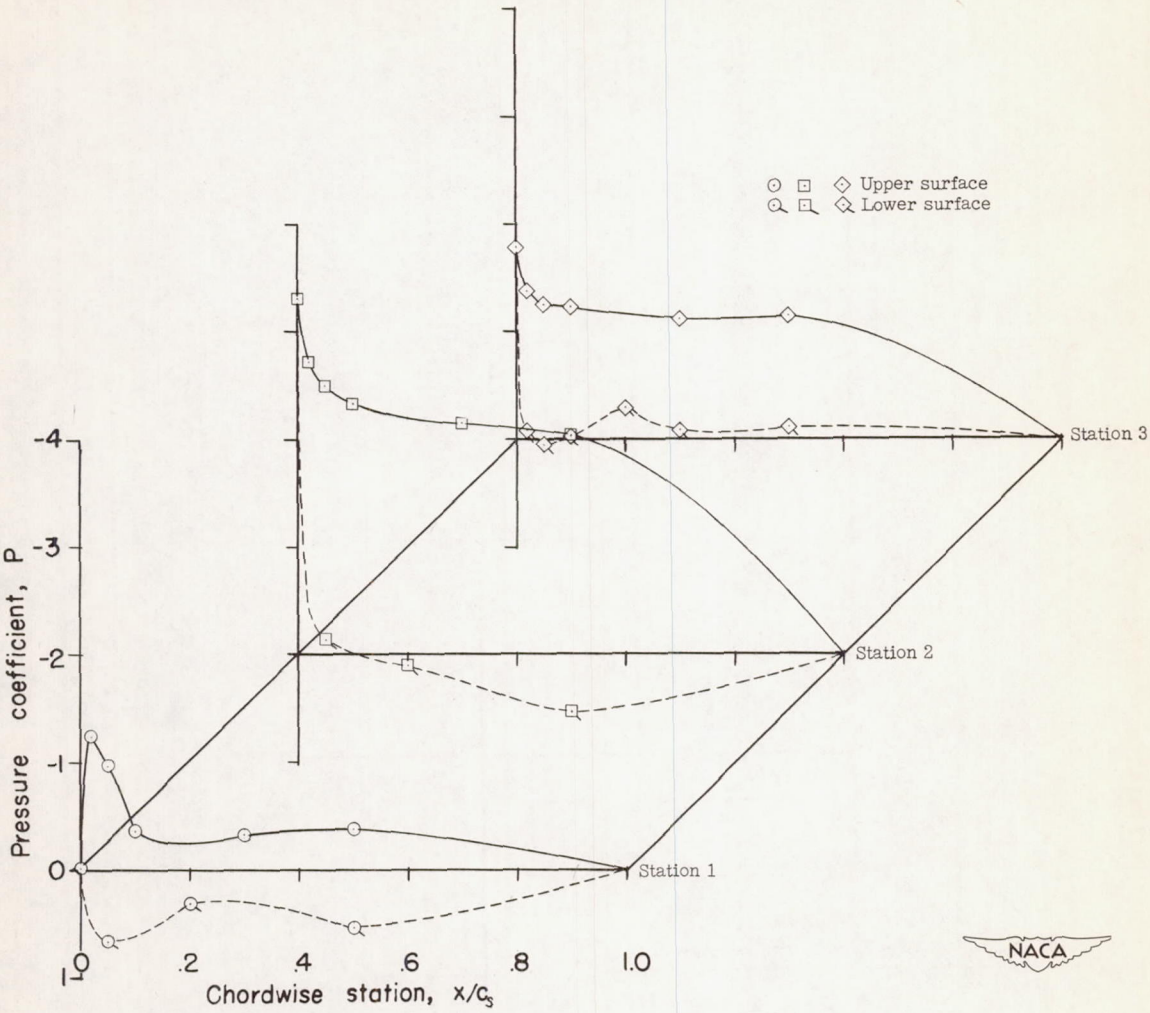
(a) $\alpha = 8.4^{\circ}$; $C_L = 0.720$.

Figure 15.- Slat chordwise pressure distributions for the 0.50b/2 slat installed on the semispan 49.1° sweptback wing with trailing-edge flap deflected. $\delta_s = 45^{\circ}$; $R = 6.1 \times 10^6$.



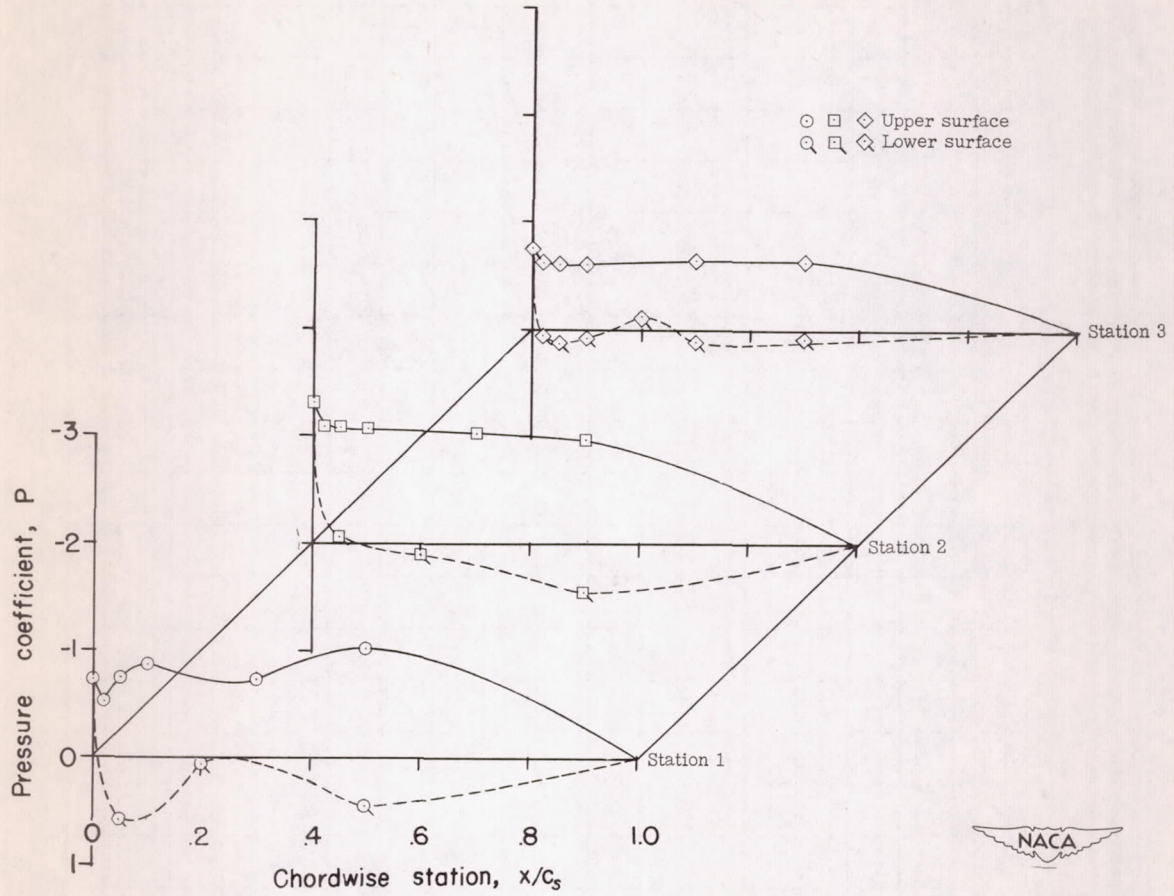
(b) $\alpha = 13.2^{\circ}$; $C_L = 0.911$.

Figure 15.- Continued.



(c) $\alpha = 19.1^{\circ}$; $C_L = 1.072$.

Figure 15.- Continued.



(d) $\alpha = 27.1^{\circ}$; $C_L = 1.020$.

Figure 15.- Concluded.

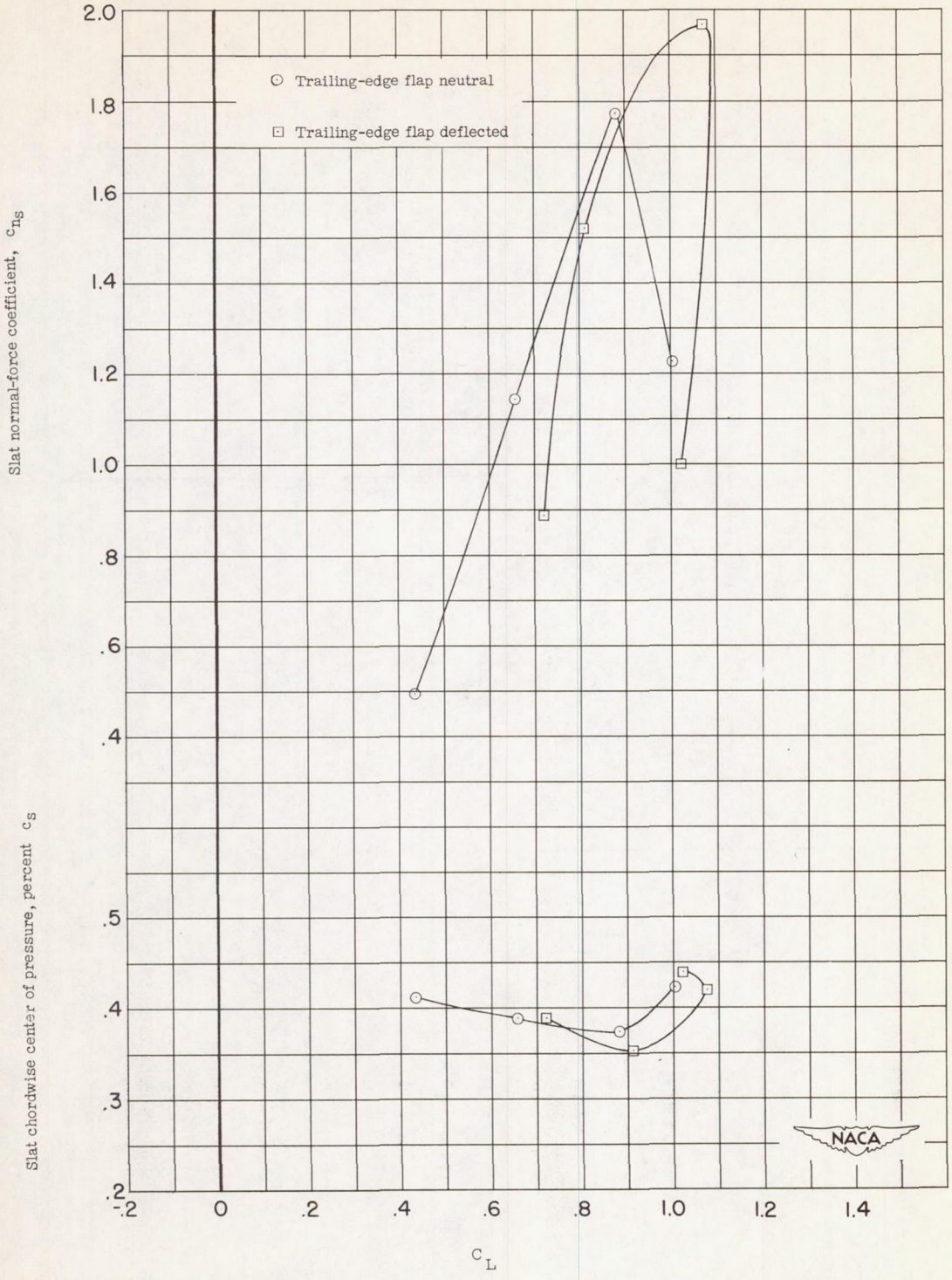


Figure 16.- Effect of trailing-edge flap deflection on the slat load characteristics for the 0.50b/2 slat installed on the semispan 49.1° sweptback wing. $\delta_s = 45°$; $R = 6.1 \times 10^6$.